

A posteriori error estimation for an augmented mixed-primal method applied to sedimentation–consolidation systems [☆]

Mario Alvarez ^a, Gabriel N. Gatica ^b, Ricardo Ruiz-Baier ^{c,*}

^a Sección de Matemática, Sede de Occidente, Universidad de Costa Rica, San Ramón de Alajuela, Costa Rica

^b CI²MA and Departamento de Ingeniería Matemática, Universidad de Concepción, Casilla 160-C, Concepción, Chile

^c Mathematical Institute, University of Oxford, A. Wiles Building, Woodstock Road, Oxford OX2 6GG, United Kingdom

ARTICLE INFO

Article history:

Received 20 October 2016

Received in revised form 19 April 2018

Accepted 21 April 2018

Available online 26 April 2018

Keywords:

Brinkman–transport coupling

Nonlinear advection–diffusion

Augmented mixed-primal formulation

Sedimentation–consolidation process

Finite element methods

A posteriori error analysis

ABSTRACT

In this paper we develop the *a posteriori* error analysis of an augmented mixed-primal finite element method for the 2D and 3D versions of a stationary flow and transport coupled system, typically encountered in sedimentation–consolidation processes. The governing equations consist in the Brinkman problem with concentration-dependent viscosity, written in terms of Cauchy pseudo-stresses and bulk velocity of the mixture; coupled with a nonlinear advection – nonlinear diffusion equation describing the transport of the solids volume fraction. We derive two efficient and reliable residual-based *a posteriori* error estimators for a finite element scheme using Raviart–Thomas spaces of order k for the stress approximation, and continuous piecewise polynomials of degree $\leq k + 1$ for both velocity and concentration. For the first estimator we make use of suitable ellipticity and inf-sup conditions together with a Helmholtz decomposition and the local approximation properties of the Clément interpolant and Raviart–Thomas operator to show its reliability, whereas the efficiency follows from inverse inequalities and localisation arguments based on triangle-bubble and edge-bubble functions. Next, we analyse an alternative error estimator, whose reliability can be proved without resorting to Helmholtz decompositions. Finally, we provide some numerical results confirming the reliability and efficiency of the estimators and illustrating the good performance of the associated adaptive algorithm for the augmented mixed-primal finite element method.

© 2018 The Author(s). Published by Elsevier Inc. This is an open access article under the CC BY license (<http://creativecommons.org/licenses/by/4.0/>).

1. Introduction

The phenomenon of gravitational sedimentation of relatively small particles within viscous fluids is of considerable importance in a number of diverse applications related for instance to wastewater treatment, mineral processing, volcanology, or hemodynamics. In this process the suspended mixture is separated into the solid particles going to the bottom of the vessel and the viscous fluid remaining on the top. Using the formalism of mixtures, one can assume that both fluid and solid phases are superimposed continua, and regarding the problem from a macroscopic viewpoint, the governing equations involving momentum and mass conservation of the phases can be conveniently recast in the form of one momentum

[☆] *Funding:* This work was partially supported by CONICYT-Chile through BASAL project PFB03 CMM, Universidad de Chile, and project Anillo ACT1118 (ANANUM); by the Ministry of Education through the project REDOC.CTA of the Graduate School, Universidad de Concepción; by Centro de Investigación en Ingeniería Matemática (CI²MA), Universidad de Concepción; and by the EPSRC through the Research Grant EP/R00207X/1.

* Corresponding author.

E-mail addresses: mario.alvarezguadamuz@ucr.ac.cr (M. Alvarez), ggatica@ci2ma.udec.cl (G.N. Gatica), ruizbaier@maths.ox.ac.uk (R. Ruiz-Baier).

and one mass equation for the mixture, together with a mass conservation equation for the solids concentration (see e.g. [10,13,35]). As the flow regime under consideration is viscous, laminar, and in the presence of a background porosity in the vessel, the PDE system under consideration consists of Brinkman equations with variable viscosity coupled with a nonlinear advection – nonlinear diffusion equation describing the transport of the volumetric fraction of the solids.

We have recently analysed in [2], the solvability of a strongly coupled flow and transport system encountered in such continuum-based models for sedimentation–consolidation processes. There we have considered the steady-state regime of the process and we have proposed an augmented variational formulation where the main unknowns given by the Cauchy pseudo-stress and bulk velocity of the mixture, and the solids volume fraction, which are sought in $\mathbb{H}(\mathbf{div}; \Omega)$, $\mathbf{H}^1(\Omega)$, and $H^1(\Omega)$, respectively. Fixed point arguments, certain regularity assumptions, and some classical results concerning variational problems and Sobolev spaces are combined to establish the solvability of the continuous and discrete coupled formulations. Consequently, the rows of the Cauchy stress tensor were approximated with Raviart–Thomas elements of order k , whereas the velocity and solids concentration were discretised with continuous piecewise polynomials of degree $\leq k + 1$. Suitable Strang-type estimates are employed to derive optimal *a priori* error estimates for the solution of the Galerkin scheme.

The purpose of this work is to provide reliable and efficient residual-based *a posteriori* error estimators for the steady sedimentation–consolidation system studied in [2]. Estimators of this kind are frequently employed to guide adaptive mesh refinement in order to guarantee an adequate convergence behaviour of the Galerkin approximations, even under the eventual presence of singularities. The global estimator η depends on local estimators η_T defined on each element T of a given mesh \mathcal{T}_h . Then, η is said to be efficient (resp. reliable) if there exists a constant $C_{\text{eff}} > 0$ (resp. $C_{\text{rel}} > 0$), independent of meshsizes, such that

$$C_{\text{eff}} \eta + \text{h.o.t.} \leq \|error\| \leq C_{\text{rel}} \eta + \text{h.o.t.},$$

where h.o.t. is a generic expression denoting one or several terms of higher order. Up to the authors knowledge, a number of *a posteriori* error estimators specifically targeted for non-viscous flow equations (e.g., Darcy) coupled with transport problems, are available in the recent literature [9,20,31,38,42]. However, only [11,32] and [3] are devoted to the *a posteriori* error analysis for coupled viscous flow-transport problems. In particular, we derive in [3], two efficient and reliable residual-based *a posteriori* error estimators for an augmented mixed-primal finite element approximation of a stationary viscous flow and transport problem, which serves as a prototype model for sedimentation–consolidation processes and other phenomena where the transport of species concentration within a viscous fluid is of interest.

In this paper, as well as in [3,4], we make use of ellipticity and inf–sup conditions together with a Helmholtz decomposition, local approximation properties of the Clément interpolant and Raviart–Thomas operator, and known estimates from [8], [22], [26], [28] and [29], to prove the reliability of a residual-based estimator. Then, inverse inequalities, the localisation technique based on triangle-bubble and edge-bubble functions imply the efficiency of the estimator. Alternatively, we deduce a second reliable and efficient residual-based *a posteriori* error estimator, where the Helmholtz decomposition is not employed in the corresponding proof of reliability. The rest of this paper is organised as follows. In Section 2, we first recall from [2] the model problem and a corresponding augmented mixed-primal formulation as well as the associated Galerkin scheme. In Section 3, we derive a reliable and efficient residual-based *a posteriori* error estimator for our Galerkin scheme. A second estimator is introduced and analysed in Section 4. Next, the analysis and results from Section 3 and 4 are extended to the three-dimensional case in Section 5. Finally, in Section 6, our theoretical results are illustrated via some numerical examples, highlighting also the good performance of the scheme and properties of the proposed error indicators.

2. The sedimentation–consolidation system

Let us denote by $\Omega \subseteq \mathbb{R}^n$, $n = 2, 3$ a given bounded domain with polyhedral boundary $\Gamma = \bar{\Gamma}_D \cup \bar{\Gamma}_N$, with $\Gamma_D \cap \Gamma_N = \emptyset$ and $|\Gamma_D|, |\Gamma_N| > 0$, and denote by \mathbf{v} the outward unit normal vector on Γ . Standard notation will be adopted for Lebesgue spaces $L^p(\Omega)$ and Sobolev spaces $H^s(\Omega)$ with norm $\|\cdot\|_{s,\Omega}$ and seminorm $|\cdot|_{s,\Omega}$. In particular, $H^{1/2}(\Gamma)$ is the space of traces of functions of $H^1(\Omega)$ and $H^{-1/2}(\Gamma)$ denotes its dual. By \mathbf{M}, \mathbb{M} we will denote the corresponding vectorial and tensorial counterparts of the generic scalar functional space M . We recall that the space

$$\mathbb{H}(\mathbf{div}; \Omega) := \{ \boldsymbol{\tau} \in \mathbb{L}^2(\Omega) : \mathbf{div} \boldsymbol{\tau} \in \mathbf{L}^2(\Omega) \},$$

equipped with the usual norm

$$\| \boldsymbol{\tau} \|_{\mathbf{div}; \Omega}^2 := \| \boldsymbol{\tau} \|_{0, \Omega}^2 + \| \mathbf{div} \boldsymbol{\tau} \|_{0, \Omega}^2$$

is a Hilbert space. As usual, \mathbb{I} stands for the identity tensor in $\mathbb{R}^{n \times n}$, and $|\cdot|$ denotes both the Euclidean norm in \mathbb{R}^n and the Frobenius norm in $\mathbb{R}^{n \times n}$.

2.1. The governing equations

The following model describes the steady state of the sedimentation–consolidation process consisting on the transport and suspension of a solid phase into an immiscible fluid contained in a vessel Ω (cf. [2]). The flow patterns are influenced by

gravity and by the local fluctuations of the solids volume fraction (see also [15,14]). After elimination of the fluid pressure (cf. [2]), namely

$$p := -\frac{1}{n} \operatorname{tr}(\boldsymbol{\sigma}),$$

the process is governed by the following system of partial differential equations:

$$\begin{aligned} \frac{1}{\mu(\phi)} \boldsymbol{\sigma}^{\text{d}} &= \nabla \mathbf{u}, \quad \mathbf{K}^{-1} \mathbf{u} - \operatorname{div} \boldsymbol{\sigma} = \mathbf{f} \phi, \quad \operatorname{div} \mathbf{u} = 0 \quad \text{in } \Omega, \\ \tilde{\boldsymbol{\sigma}} &= \vartheta(\phi) \nabla \phi - \phi \mathbf{u} - f_{\text{bk}}(\phi) \mathbf{k}, \quad \beta \phi - \operatorname{div} \tilde{\boldsymbol{\sigma}} = g \quad \text{in } \Omega, \end{aligned} \tag{2.1}$$

along with the following boundary conditions:

$$\begin{aligned} \mathbf{u} &= \mathbf{u}_D \quad \text{on } \Gamma_D, \quad \boldsymbol{\sigma} \mathbf{v} = \mathbf{0} \quad \text{on } \Gamma_N, \\ \phi &= 0 \quad \text{on } \Gamma_D, \quad \text{and } \tilde{\boldsymbol{\sigma}} \cdot \mathbf{v} = 0 \quad \text{on } \Gamma_N, \end{aligned} \tag{2.2}$$

where $(\cdot)^{\text{d}}$ denotes the deviatoric operator. The sought quantities are the Cauchy fluid pseudo-stress $\boldsymbol{\sigma}$, the average velocity of the mixture \mathbf{u} , and the volumetric fraction of the solids (in short, concentration) ϕ . In this context, the parameter β is a positive constant representing the porosity of the medium, and the permeability tensor $\mathbf{K} \in \mathbb{C}(\bar{\Omega}) := [C(\bar{\Omega})]^{n \times n}$ and its inverse are symmetric and uniformly positive definite, which means that there exists $\alpha_K > 0$ such that

$$\mathbf{v}^{\text{t}} \mathbf{K}^{-1}(\mathbf{x}) \mathbf{v} \geq \alpha_K |\mathbf{v}|^2 \quad \forall \mathbf{v} \in \mathbb{R}^n, \quad \forall \mathbf{x} \in \Omega.$$

Here, we assume that the kinematic effective viscosity, μ ; the one-directional Kynch batch flux density function describing hindered settling, f_{bk} ; and the diffusion or sediment compressibility, ϑ ; are nonlinear scalar functions of the concentration ϕ . In turn, \mathbf{k} is a vector pointing in the direction of gravity and $\mathbf{f} \in \mathbf{L}^\infty(\Omega)$, $\mathbf{u}_D \in \mathbf{H}^{1/2}(\Gamma_D)$, $g \in L^2(\Omega)$ are given functions. For sake of the subsequent analysis, the Dirichlet datum for the concentration will be assumed homogeneous $\phi_D = 0$; ϑ is assumed of class C^1 ; and we suppose that there exist positive constants $\mu_1, \mu_2, \gamma_1, \gamma_2, \vartheta_1, \vartheta_2, L_\mu, L_\vartheta$, and L_f , such that for each $s, t \in \mathbb{R}$ there holds

$$\mu_1 \leq \mu(s) \leq \mu_2, \quad \gamma_1 \leq f_{\text{bk}}(s) \leq \gamma_2, \quad \vartheta_1 \leq \vartheta(s) \leq \vartheta_2, \tag{2.3}$$

$$|\mu(s) - \mu(t)| \leq L_\mu |s - t|, \quad |\vartheta(s) - \vartheta(t)| \leq L_\vartheta |s - t|, \quad \text{and } |f_{\text{bk}}(s) - f_{\text{bk}}(t)| \leq L_f |s - t|. \tag{2.4}$$

We end this section by highlighting, as in [2] and [5], that the main advantage of using a mixed formulation in the fluid equations has to do with the eventual need of approximating other variables of physical interest, such as some components of the fluid stress tensor, the gradient of velocity, and the vorticity. Indeed, it is clear from (2.1) that $\nabla \mathbf{u}$ and the vorticity $\boldsymbol{\gamma}(\mathbf{u}) := \frac{1}{2} (\nabla \mathbf{u} - (\nabla \mathbf{u})^{\text{t}})$, can both be computed explicitly in terms of $\boldsymbol{\sigma}$ and ϕ , as $\frac{1}{\mu(\phi)} \boldsymbol{\sigma}^{\text{d}}$ and $\frac{1}{2\mu(\phi)} (\boldsymbol{\sigma}^{\text{d}} - (\boldsymbol{\sigma}^{\text{d}})^{\text{t}})$, respectively, where the superscript t stands from now for the transpose of a matrix. In this way, and as we stress below in Section 2.3, these further unknowns are approximated directly, without resorting to any numerical differentiation of the discrete velocity field, thus avoiding the significative loss in accuracy caused by this procedure. Other mixed-primal formulations for Brinkman-transport systems using vorticity as additional unknown in the flow equations can be found in e.g. [7,33].

2.2. The augmented mixed-primal formulation

The homogeneous Neumann and Dirichlet boundary conditions for $\boldsymbol{\sigma}$ on Γ_N and ϕ on Γ_D (second and third relations of (2.2), respectively) suggest the introduction of the following functional spaces

$$\begin{aligned} \mathbb{H}_N(\operatorname{div}; \Omega) &:= \left\{ \boldsymbol{\tau} \in \mathbb{H}(\operatorname{div}; \Omega) : \boldsymbol{\tau} \mathbf{v} = \mathbf{0} \quad \text{on } \Gamma_N \right\}, \\ H_{\Gamma_D}^1(\Omega) &:= \left\{ \psi \in H^1(\Omega) : \psi = 0 \quad \text{on } \Gamma_D \right\}. \end{aligned}$$

Consequently, an augmented mixed-primal formulation for our original coupled problem (2.1) reads as follows: Find $(\boldsymbol{\sigma}, \mathbf{u}, \phi) \in \mathbb{H}_N(\operatorname{div}; \Omega) \times \mathbf{H}^1(\Omega) \times H_{\Gamma_D}^1(\Omega)$ such that

$$\begin{aligned} B_\phi((\boldsymbol{\sigma}, \mathbf{u}), (\boldsymbol{\tau}, \mathbf{v})) &= F_\phi(\boldsymbol{\tau}, \mathbf{v}) \quad \forall (\boldsymbol{\tau}, \mathbf{v}) \in \mathbb{H}_N(\operatorname{div}; \Omega) \times \mathbf{H}^1(\Omega), \\ A_{\mathbf{u}}(\phi, \psi) &= G_\phi(\psi) \quad \forall \psi \in H_{\Gamma_D}^1(\Omega), \end{aligned} \tag{2.5}$$

where

$$B_\phi((\boldsymbol{\sigma}, \mathbf{u}), (\boldsymbol{\tau}, \mathbf{v})) := \int_\Omega \frac{1}{\mu(\phi)} \boldsymbol{\sigma}^d : \boldsymbol{\tau}^d + \int_\Omega \mathbf{u} \cdot \mathbf{div} \boldsymbol{\tau} - \int_\Omega \mathbf{v} \cdot \mathbf{div} \boldsymbol{\sigma} + \int_\Omega \mathbf{K}^{-1} \mathbf{u} \cdot \mathbf{v} \tag{2.6}$$

$$+ \kappa_1 \int_\Omega \left(\nabla \mathbf{u} - \frac{1}{\mu(\phi)} \boldsymbol{\sigma}^d \right) : \nabla \mathbf{v} - \kappa_2 \int_\Omega \mathbf{K}^{-1} \mathbf{u} \cdot \mathbf{div} \boldsymbol{\tau} + \kappa_2 \int_\Omega \mathbf{div} \boldsymbol{\sigma} \cdot \mathbf{div} \boldsymbol{\tau},$$

$$F_\phi(\boldsymbol{\tau}, \mathbf{v}) := \langle \boldsymbol{\tau} \mathbf{v}, \mathbf{u}_D \rangle_{\Gamma_D} + \int_\Omega \mathbf{f} \phi \cdot \mathbf{v} - \kappa_2 \int_\Omega \mathbf{f} \phi \cdot \mathbf{div} \boldsymbol{\tau},$$

$$A_{\mathbf{u}}(\phi, \psi) := \int_\Omega \vartheta(\phi) \nabla \phi \cdot \nabla \psi - \int_\Omega \phi \mathbf{u} \cdot \nabla \psi + \int_\Omega \beta \phi \psi \quad \forall \phi, \psi \in H^1_{\Gamma_D}(\Omega), \tag{2.7}$$

$$G_\phi(\psi) := \int_\Omega \mathbf{f}_{bk}(\phi) \mathbf{k} \cdot \nabla \psi + \int_\Omega g \psi \quad \forall \psi \in H^1_{\Gamma_D}(\Omega),$$

and κ_1, κ_2 are positive parameters satisfying $\kappa_1 \in \left(0, \frac{2\delta\mu_1}{\mu_2}\right)$ and $\kappa_2 \in \left(0, \frac{2\tilde{\delta}\alpha\kappa}{n\|\mathbf{K}^{-1}\|_\infty}\right)$, with $\delta \in (0, 2\mu_1)$ and $\tilde{\delta} \in \left(0, \frac{2}{n\|\mathbf{K}^{-1}\|_\infty}\right)$. Further details yielding the weak formulation (2.5), along with its fixed-point based solvability analysis can be found in [2, Section 3]. Nevertheless, some remarks concerning (2.5), and particularly regarding the resulting bilinear forms B_ϕ (cf. (2.6)) and $A_{\mathbf{u}}$ (cf. (2.7)), are worth of being given in what follows.

First of all, we observe that, due to the use of a mixed formulation in the Brinkman problem, the Dirichlet boundary condition for the velocity of the fluid becomes a natural one since it appears automatically when integrating by parts the right hand side of the corresponding constitutive law (first equation in (2.1)). As a consequence, there is no need of imposing it weakly as would have been the case if a primal (instead of a dual-mixed) formulation were used, or when the dual-mixed approach is kept, but a Neumann boundary condition (normal component of $\boldsymbol{\sigma}$) is prescribed instead of the Dirichlet one. Similar comments hold for the transport equation. In fact, since a primal formulation is employed there, the homogeneous Dirichlet boundary condition for the concentration is simply incorporated into the definition of the space $H^1_{\Gamma_D}(\Omega)$ where this unknown lives. However, if it were non-homogeneous and the primal approach is kept, it would become essential, and hence a weak imposition of it would be necessary. Alternatively, one may switch to a dual-mixed formulation for the transport equation as well since in this case a non-homogeneous Dirichlet boundary condition becomes natural.

On the other hand, it is also important to emphasise here the relevance of the augmentation procedure for our analysis. In this regard, we first recall from [2, Section 3.1] that in order to estimate the second term defining $A_{\mathbf{u}}$ (cf. (2.7)), which is used to derive the solvability of the transport equation (second row of (2.5)), we need that \mathbf{u} lies in $\mathbf{H}^1(\Omega)$. Indeed, this requirement arises naturally after applying the Cauchy–Schwarz inequality and the compact imbedding of $\mathbf{H}^1(\Omega)$ into $\mathbf{L}^4(\Omega)$ to that term. Hence, the incorporation of the identities given by the first two equations of (2.1), but tested differently, namely

$$\kappa_1 \int_\Omega \left(\nabla \mathbf{u} - \frac{1}{\mu(\phi)} \boldsymbol{\sigma}^d \right) : \nabla \mathbf{v} = 0 \quad \forall \mathbf{v} \in \mathbf{H}^1(\Omega), \tag{2.8}$$

and

$$\kappa_2 \left(\int_\Omega \mathbf{K}^{-1} \mathbf{u} \cdot \mathbf{div} \boldsymbol{\tau} - \int_\Omega \mathbf{div} \boldsymbol{\sigma} \cdot \mathbf{div} \boldsymbol{\tau} \right) = \kappa_2 \int_\Omega \mathbf{f} \phi \cdot \mathbf{div} \boldsymbol{\tau} \quad \forall \boldsymbol{\tau} \in \mathbb{H}_N(\mathbf{div}; \Omega), \tag{2.9}$$

is crucial for concluding the ellipticity of the bilinear form B_ϕ (cf. [2, proof of Lemma 3.3]) precisely with respect to the $\mathbb{H}(\mathbf{div}; \Omega) \times \mathbf{H}^1(\Omega)$ norm, thus guaranteeing Galerkin stability and the associated a priori error estimates in the same product norm. Alternatively, a discontinuous Galerkin type scheme could also be employed, which anyway is matter of a separate work, but we advance that in this case stability with respect to the $\mathbb{L}^2(\Omega) \times \mathbf{L}^2(\Omega)$ norm only would be obtained.

Furthermore, we remark that a by-side cost of the ellipticity for B_ϕ is the lack of symmetry of this bilinear form, which, besides of a couple of different signs on the right-hand side of (2.6), is mainly caused by the second and first term on the left-hand sides of (2.8) and (2.9), respectively. In other words, either we have symmetry or ellipticity for B_ϕ but not both, and we opted for the latter because of the consequent flexibility in choosing the finite element subspaces, fact that is further explained below at the end of Section 2.3.

Finally, we notice that while no additional stabilisation is imposed on the transport equation, our analysis is certainly restricted to the assumptions on the diffusion coefficient ϑ , namely the upper and lower bounds given in (2.3) and the Lipschitz–continuity hypothesis stated in (2.4). If we faced a case of very small ϑ , which would also be matter of a separate work, then probably suitable stabilising terms would need to be added to the corresponding formulation.

2.3. The augmented mixed-primal finite element method

We denote by \mathcal{T}_h a regular partition of Ω into triangles T (resp. tetrahedra T in \mathbb{R}^3) of diameter h_T , and meshsize $h := \max\{h_T : T \in \mathcal{T}_h\}$. In addition, given an integer $k \geq 0$, $\mathbf{P}_k(T)$ denotes the space of polynomial functions on T of degree $\leq k$, and we define the corresponding local Raviart–Thomas space of order k as $\mathbf{RT}_k(T) := \mathbf{P}_k(T) \oplus \mathbf{P}_k(T)\mathbf{x}$, where, according to the notations described in Section 1, $\mathbf{P}_k(T) = [\mathbf{P}_k(T)]^n$, and $\mathbf{x} \in \mathbb{R}^n$. Then, the Galerkin scheme associated to (2.5), corresponds to: Find $(\boldsymbol{\sigma}_h, \mathbf{u}_h, \phi_h) \in \mathbb{H}_h^\boldsymbol{\sigma} \times \mathbf{H}_h^\mathbf{u} \times H_h^\phi$ such that

$$\begin{aligned} B_{\phi_h}((\boldsymbol{\sigma}_h, \mathbf{u}_h), (\boldsymbol{\tau}_h, \mathbf{v}_h)) &= F_{\phi_h}(\boldsymbol{\tau}_h, \mathbf{v}_h) \quad \forall (\boldsymbol{\tau}_h, \mathbf{v}_h) \in \mathbb{H}_h^\boldsymbol{\sigma} \times \mathbf{H}_h^\mathbf{u}, \\ A_{\mathbf{u}_h}(\phi_h, \psi_h) &= \int_{\Omega} f_{bk}(\phi_h) \mathbf{k} \cdot \nabla \psi_h + \int_{\Omega} g \psi_h \quad \forall \psi_h \in H_h^\phi, \end{aligned} \tag{2.10}$$

where the involved finite element spaces are defined as

$$\begin{aligned} \mathbb{H}_h^\boldsymbol{\sigma} &:= \left\{ \boldsymbol{\tau}_h \in \mathbb{H}_N(\mathbf{div}; \Omega) : \mathbf{c}^\top \boldsymbol{\tau}_h|_T \in \mathbf{RT}_k(T) \quad \forall \mathbf{c} \in \mathbb{R}^n, \quad \forall T \in \mathcal{T}_h \right\}, \\ \mathbf{H}_h^\mathbf{u} &:= \left\{ \mathbf{v}_h \in \mathbf{C}(\overline{\Omega}) : \mathbf{v}_h|_T \in \mathbf{P}_{k+1}(T) \quad \forall T \in \mathcal{T}_h \right\}, \\ H_h^\phi &:= \left\{ \psi_h \in C(\overline{\Omega}) \cap H_{\Gamma_D}^1(\Omega) : \psi_h|_T \in \mathbf{P}_{k+1}(T) \quad \forall T \in \mathcal{T}_h \right\}. \end{aligned} \tag{2.11}$$

The solvability analysis and a priori error estimates for (2.10) have been derived in [2, Section 5]. In turn, as already announced in Section 2.1, we stress here that numerical approximations p_h , $(\nabla \mathbf{u})_h$, and $\boldsymbol{\gamma}(\mathbf{u})_h$ of the pressure, the gradient of velocity, and the vorticity, respectively, are easily obtained through the following postprocessed formulae depending only on $\boldsymbol{\sigma}_h$ and ϕ_h :

$$p_h := -\frac{1}{n} \text{tr}(\boldsymbol{\sigma}_h), \quad (\nabla \mathbf{u})_h := \frac{1}{\mu(\phi_h)} \boldsymbol{\sigma}_h^d, \quad \text{and} \quad \boldsymbol{\gamma}(\mathbf{u})_h := \frac{1}{2\mu(\phi_h)} (\boldsymbol{\sigma}_h^d - (\boldsymbol{\sigma}_h^d)^\top).$$

Moreover, it is easy to prove that in this case there exist positive constants C_1 , C_2 , and C_3 , depending on n , μ_1 , and L_μ , such that, under the reasonable assumption that $\boldsymbol{\sigma} \in \mathbb{L}^4(\Omega)$, the following a priori error estimates hold

$$\begin{aligned} \|p - p_h\|_{0,\Omega} &\leq C_1 \|\boldsymbol{\sigma} - \boldsymbol{\sigma}_h\|_{0,\Omega}, \\ \|\nabla \mathbf{u} - (\nabla \mathbf{u})_h\|_{0,\Omega} &\leq C_2 \left\{ \|\boldsymbol{\sigma} - \boldsymbol{\sigma}_h\|_{0,\Omega} + \|\phi - \phi_h\|_{1,\Omega} \|\boldsymbol{\sigma}\|_{\mathbb{L}^4(\Omega)} \right\}, \end{aligned}$$

and

$$\|\boldsymbol{\gamma}(\mathbf{u}) - \boldsymbol{\gamma}(\mathbf{u})_h\|_{0,\Omega} \leq C_3 \left\{ \|\boldsymbol{\sigma} - \boldsymbol{\sigma}_h\|_{0,\Omega} + \|\phi - \phi_h\|_{1,\Omega} \|\boldsymbol{\sigma}\|_{\mathbb{L}^4(\Omega)} \right\},$$

thus showing that the rates of convergence attained by $\boldsymbol{\sigma}_h$ and ϕ_h imply those of the aforescribed approximations for the additional unknowns.

At this point we also notice that another important consequence of the augmentation is given by the fact – guaranteed by the ellipticity of B_ϕ – that, not only the ones defined in (2.11), but any pair of finite element subspaces $\mathbb{H}_h^\boldsymbol{\sigma}$ and $\mathbf{H}_h^\mathbf{u}$ of $\mathbb{H}_N(\mathbf{div}; \Omega)$ and $\mathbf{H}^1(\Omega)$, respectively, will yield the stability of (2.10). Otherwise, if instead of ellipticity the bilinear form B_ϕ is chosen to be symmetric, then most likely it will be able to satisfy just continuous and discrete global inf-sup conditions, and hence not all the possible finite element subspaces but only some specific ones will be eligible for guaranteeing a stable Galerkin scheme.

3. A residual-based a posteriori error estimator

In this section we introduce a reliable and efficient residual-based *a posteriori* error estimator for the Galerkin scheme (2.10). In particular, as well as in [3], a Helmholtz decomposition will be employed in the corresponding proof of reliability. Even if this analysis will be restricted to the two-dimensional case using the discrete spaces from Section 2.3, an extension to the 3D case will be addressed in detail in Section 5, below.

Given a suitably chosen $r > 0$ (see [2] for details), we define the balls

$$W := \{\phi \in H_{\Gamma_D}^1(\Omega) : \|\phi\|_{1,\Omega} \leq r\} \quad \text{and} \quad W_h := \{\phi_h \in H_h^\phi : \|\phi_h\|_{1,\Omega} \leq r\}, \tag{3.1}$$

and throughout the rest of the paper we let $(\boldsymbol{\sigma}, \mathbf{u}, \phi) \in \mathbb{H}_N(\mathbf{div}; \Omega) \times \mathbf{H}^1(\Omega) \times H_{\Gamma_D}^1(\Omega)$ with $\phi \in W$ and $(\boldsymbol{\sigma}_h, \mathbf{u}_h, \phi_h) \in \mathbb{H}_h^\boldsymbol{\sigma} \times \mathbf{H}_h^\mathbf{u} \times H_h^\phi$ with $\phi_h \in W_h$ be the solutions of the continuous and discrete formulations (2.5) and (2.10), respectively. In addition, we set

$$H := \mathbb{H}_N(\mathbf{div}, \Omega) \times \mathbf{H}^1(\Omega), \quad \|(\boldsymbol{\tau}, \mathbf{v})\|_H := \|\boldsymbol{\tau}\|_{\mathbf{div};\Omega} + \|\mathbf{v}\|_{1,\Omega} \quad \forall (\boldsymbol{\tau}, \mathbf{v}) \in H,$$

and recall from [2, Theorems 3.13 and 4.7] that the following a priori estimates hold

$$\begin{aligned} \|(\boldsymbol{\sigma}, \mathbf{u})\|_H &\leq C_S \left\{ \|\mathbf{u}_D\|_{1/2,\Gamma_D} + \|\phi\|_{1,\Omega} \|\mathbf{f}\|_{\infty,\Omega} \right\}, \\ \|(\boldsymbol{\sigma}_h, \mathbf{u}_h)\|_H &\leq C_S \left\{ \|\mathbf{u}_D\|_{1/2,\Gamma_D} + \|\phi_h\|_{1,\Omega} \|\mathbf{f}\|_{\infty,\Omega} \right\}, \end{aligned}$$

where C_S is a positive constant independent of ϕ and ϕ_h .

3.1. The local error indicator

Given $T \in \mathcal{T}_h$, we let $\mathcal{E}_h(T)$ be the set of its edges, and let \mathcal{E}_h be the set of all edges of the triangulation \mathcal{T}_h . Then we write $\mathcal{E}_h = \mathcal{E}_h(\Omega) \cup \mathcal{E}_h(\Gamma_D) \cup \mathcal{E}_h(\Gamma_N)$, where $\mathcal{E}_h(\Omega) := \{e \in \mathcal{E}_h : e \subseteq \Omega\}$, $\mathcal{E}_h(\Gamma_D) := \{e \in \mathcal{E}_h : e \subseteq \Gamma_D\}$ and $\mathcal{E}_h(\Gamma_N) := \{e \in \mathcal{E}_h : e \subseteq \Gamma_N\}$. Also, for each edge $e \in \mathcal{E}_h$ we fix a unit normal vector $\mathbf{v}_e := (v_1, v_2)^\top$, and let $\mathbf{s}_e := (-v_2, v_1)^\top$ be the corresponding fixed unit tangential vector along e . Then, given $e \in \mathcal{E}_h(\Omega)$ and $\mathbf{v} \in \mathbf{L}^2(\Omega)$ such that $\mathbf{v}|_T \in \mathbf{C}(T)$ on each $T \in \mathcal{T}_h$, we let $\llbracket \mathbf{v} \cdot \mathbf{v}_e \rrbracket$ be the corresponding jump across e , that is, $\llbracket \mathbf{v} \cdot \mathbf{v}_e \rrbracket := (\mathbf{v}|_T - \mathbf{v}|_{T'}) \cdot \mathbf{v}_e$, where T and T' are the triangles of \mathcal{T}_h having e as a common edge. Similarly, given a tensor field $\boldsymbol{\tau} \in \mathbb{L}^2(\Omega)$ such that $\boldsymbol{\tau}|_T \in \mathbb{C}(T)$ on each $T \in \mathcal{T}_h$, we let $\llbracket \boldsymbol{\tau} \mathbf{s}_e \rrbracket$ be the corresponding jump across e , that is, $\llbracket \boldsymbol{\tau} \mathbf{s}_e \rrbracket := (\boldsymbol{\tau}|_T - \boldsymbol{\tau}|_{T'}) \cdot \mathbf{s}_e$. If no confusion arises, we will simply write \mathbf{s} and \mathbf{v} instead \mathbf{s}_e and \mathbf{v}_e , respectively.

Moreover, given scalar, vector, and tensor valued fields $v, \boldsymbol{\varphi} := (\varphi_1, \varphi_2)$ and $\boldsymbol{\tau} := (\tau_{ij})$, respectively, we denote

$$\mathbf{curl}(v) := \begin{pmatrix} \frac{\partial v}{\partial x_2} \\ -\frac{\partial v}{\partial x_1} \end{pmatrix}, \quad \mathbf{curl}(\boldsymbol{\varphi}) := \begin{pmatrix} \mathbf{curl}(\varphi_1)^\top \\ \mathbf{curl}(\varphi_2)^\top \end{pmatrix}, \quad \text{and} \quad \mathbf{curl}(\boldsymbol{\tau}) := \begin{pmatrix} \frac{\partial \tau_{12}}{\partial x_1} - \frac{\partial \tau_{11}}{\partial x_2} \\ \frac{\partial \tau_{22}}{\partial x_1} - \frac{\partial \tau_{21}}{\partial x_2} \end{pmatrix}.$$

Then we let $\tilde{\boldsymbol{\sigma}}_h := \vartheta(\phi_h)\nabla\phi_h - \phi_h\mathbf{u}_h - f_{bk}(\phi_h)\mathbf{k}$ and define for each $T \in \mathcal{T}_h$ a local error indicator as follows

$$\begin{aligned} \theta_T^2 &:= \|\mathbf{f}\phi_h - (\mathbf{K}^{-1}\mathbf{u}_h - \mathbf{div}\boldsymbol{\sigma}_h)\|_{0,T}^2 + \left\| \nabla\mathbf{u}_h - \frac{1}{\mu(\phi_h)}\boldsymbol{\sigma}_h^d \right\|_{0,T}^2 + h_T^2 \|g - (\beta\phi_h - \mathbf{div}\tilde{\boldsymbol{\sigma}}_h)\|_{0,T}^2 \\ &+ h_T^2 \left\| \mathbf{curl} \left\{ \frac{1}{\mu(\phi_h)}\boldsymbol{\sigma}_h^d \right\} \right\|_{0,T}^2 + \sum_{e \in \mathcal{E}_h(T) \cap \mathcal{E}_h(\Omega)} h_e \left\| \left\llbracket \frac{1}{\mu(\phi_h)}\boldsymbol{\sigma}_h^d \mathbf{s} \right\rrbracket \right\|_{0,e}^2 \\ &+ \sum_{e \in \mathcal{E}_h(T) \cap \mathcal{E}_h(\Omega)} h_e \|\llbracket \tilde{\boldsymbol{\sigma}}_h \cdot \mathbf{v}_e \rrbracket\|_{0,e}^2 + \sum_{e \in \mathcal{E}_h(T) \cap \mathcal{E}_h(\Gamma_N)} h_e \|\tilde{\boldsymbol{\sigma}}_h \cdot \mathbf{v}\|_{0,e}^2 \\ &+ \sum_{e \in \mathcal{E}_h(T) \cap \mathcal{E}_h(\Gamma_D)} \|\mathbf{u}_D - \mathbf{u}_h\|_{0,e}^2 + \sum_{e \in \mathcal{E}_h(T) \cap \mathcal{E}_h(\Gamma_D)} h_e \left\| \frac{d\mathbf{u}_D}{ds} - \frac{1}{\mu(\phi_h)}\boldsymbol{\sigma}_h^d \mathbf{s} \right\|_{0,e}^2. \end{aligned} \tag{3.2}$$

We remark that the last term defining θ_T^2 requires that $\frac{d\mathbf{u}_D}{ds}|_e \in \mathbf{L}^2(e)$ for each $e \in \mathcal{E}_h(\Gamma_D)$. This is fixed by assuming from now on that $\mathbf{u}_D \in \mathbf{H}_0^1(\Gamma_D)$. In turn, it is not difficult to see that each term defining θ_T^2 has a residual character, and hence, proceeding as usual, a global residual error estimator can be defined as

$$\boldsymbol{\theta} := \left\{ \sum_{T \in \mathcal{T}_h} \theta_T^2 \right\}^{1/2}. \tag{3.3}$$

3.2. Reliability

Throughout the rest of the paper we assume that Γ_N is contained in the boundary of a convex extension of Ω , that is, there exists a convex domain B such that $\Omega \subseteq B$ and $\Gamma_N \subseteq \partial B$ (see, e.g. [25, Theorem 3.2 and Figure 3.1]). Furthermore, according to the regularity estimate given in [2, eq. (3.24)], we also suppose from now on that $g \in H^{\delta}(\Omega)$ for some $\delta \in (0, 1)$. Then the main result of this section is stated as follows.

Theorem 3.1. Assume that Ω is a connected domain and that \mathbf{u}_D, Γ_N , and g are as stated above. In addition, assume that the data $\mathbf{k}, g, \vartheta, \mathbf{u}_D$, and \mathbf{f} are sufficiently small so that there holds

$$C_4 |\mathbf{k}| + C_5 \|g\|_{\delta,\Omega} + C_6 \vartheta + C_7 \|\mathbf{u}_D\|_{1/2+\delta,\Gamma_D} + C_8 \|\mathbf{f}\|_{\infty,\Omega} < \frac{1}{2}, \tag{3.4}$$

where the involved constants are made precise in (3.12), below. Then, there exists a constant $C_{\text{rel}} > 0$, which depends only on the model parameters, on $\|\mathbf{u}_D\|_{1/2+\delta, \Gamma_D}$, $\|\mathbf{f}\|_{\infty, \Omega}$, and possibly other constants, but all independent of h , such that

$$\|\phi - \phi_h\|_{1, \Omega} + \|(\boldsymbol{\sigma}, \mathbf{u}) - (\boldsymbol{\sigma}_h, \mathbf{u}_h)\|_H \leq C_{\text{rel}} \boldsymbol{\theta}. \tag{3.5}$$

A couple of preliminary estimates aiming to prove (3.5) are given in the following two subsections.

3.2.1. A preliminary estimate for the stress and velocity error

In order to simplify the subsequent writing, we introduce in advance the following constants

$$C_0 := \frac{1}{\alpha(\Omega)}, \quad C_1 := 2C_0 C_\delta \tilde{C}_\delta \widehat{C}_S(r) \frac{L\mu(1 + \kappa_1^2)^{1/2}}{\mu_1^2}, \quad C_2 := C_0(1 + \kappa_2^2)^{1/2} + rC_1, \tag{3.6}$$

where $\widehat{C}_S(r)$ and $C_\delta, \tilde{C}_\delta$ are defined in [2, eq. (3.23)] and [2, Lemma 3.6 and Theorem 3.10], respectively.

Lemma 3.2. Let $\boldsymbol{\theta}_0^2 := \sum_{T \in \mathcal{T}_h} \theta_{0,T}^2$, where for each $T \in \mathcal{T}_h$ we set

$$\theta_{0,T}^2 := \|\mathbf{f}\phi_h - (\mathbf{K}^{-1}\mathbf{u}_h - \mathbf{div}\boldsymbol{\sigma}_h)\|_{0,T}^2 + \left\| \nabla\mathbf{u}_h - \frac{1}{\mu(\phi_h)}\boldsymbol{\sigma}_h^d \right\|_{0,T}^2. \tag{3.7}$$

Then there exists $\bar{C} > 0$, depending on C_0, κ_1 , such that

$$\|(\boldsymbol{\sigma}, \mathbf{u}) - (\boldsymbol{\sigma}_h, \mathbf{u}_h)\|_H \leq \bar{C} \left\{ \boldsymbol{\theta}_0 + \|E_h\|_{\mathbb{H}_N(\mathbf{div}, \Omega)'} \right\} + \left\{ C_1 \|\mathbf{u}_D\|_{1/2+\delta, \Gamma_D} + C_2 \|\mathbf{f}\|_{\infty, \Omega} \right\} \|\phi - \phi_h\|_{1, \Omega}, \tag{3.8}$$

where C_1 and C_2 are given by (3.6), and the functional $E_h \in \mathbb{H}_N(\mathbf{div}, \Omega)'$ is defined by

$$\begin{aligned} E_h(\boldsymbol{\zeta}) := & \langle \boldsymbol{\zeta} \mathbf{v}, \mathbf{u}_D \rangle_{\Gamma_D} - \int_{\Omega} \frac{1}{\mu(\phi_h)} \boldsymbol{\sigma}_h^d : \boldsymbol{\zeta} - \int_{\Omega} \mathbf{u}_h \cdot \mathbf{div}\boldsymbol{\zeta} \\ & - \kappa_2 \int_{\Omega} (\mathbf{f}\phi_h - (\mathbf{K}^{-1}\mathbf{u}_h - \mathbf{div}\boldsymbol{\sigma}_h)) \cdot \mathbf{div}\boldsymbol{\zeta} \quad \forall \boldsymbol{\zeta} \in \mathbb{H}_N(\mathbf{div}, \Omega). \end{aligned} \tag{3.9}$$

In addition, there holds

$$E_h(\boldsymbol{\zeta}_h) = 0 \quad \forall \boldsymbol{\zeta}_h \in \mathbb{H}_h^\sigma. \tag{3.10}$$

Proof. Even though the present bilinear form B_ϕ (cf. (2.6)) and the corresponding one from [3, eq. (2.9)] differ in a couple of linear terms, the present proof is almost verbatim as [3, Lemma 3.2], particularly concerning the application of the H -ellipticity (see [2, Lemma 3.3]) of B_ϕ to the error $(\boldsymbol{\sigma}, \mathbf{u}) - (\boldsymbol{\sigma}_h, \mathbf{u}_h)$, and the estimates for $|B_{\phi_h}(\cdot, (\boldsymbol{\zeta}, \mathbf{w})) - B_\phi(\cdot, (\boldsymbol{\zeta}, \mathbf{w}))|$ and $|F_\phi(\boldsymbol{\zeta}, \mathbf{w}) - F_{\phi_h}(\boldsymbol{\zeta}, \mathbf{w})|$, and hence further details are omitted. \square

Observe, according to (3.10), that for each $\boldsymbol{\zeta} \in \mathbb{H}_N(\mathbf{div}, \Omega)$ we can write

$$E_h(\boldsymbol{\zeta}) = E_h(\boldsymbol{\zeta} - \boldsymbol{\zeta}_h) \quad \forall \boldsymbol{\zeta}_h \in \mathbb{H}_h^\sigma,$$

and hence the upper bound of $\|E_h\|_{\mathbb{H}_N(\mathbf{div}, \Omega)'}$ to be derived below (see Section 3.2.3) will employ the foregoing expression with a suitable choice of $\boldsymbol{\zeta}_h \in \mathbb{H}_h^\sigma$.

We end this section with an alternative expression for the functional E_h , which will be used later on in Section 3.2.4 to obtain a partial estimate for $\|E_h\|_{\mathbb{H}_N(\mathbf{div}, \Omega)'}$, and then in Section 4 to derive a second *a posteriori* error estimator. In fact, integrating by parts the expression $\int_{\Omega} \mathbf{u}_h \cdot \mathbf{div}\boldsymbol{\zeta}$, and using the homogeneous Neumann boundary condition on Γ_N , we find that E_h can be rewritten as

$$\begin{aligned} E_h(\boldsymbol{\zeta}) := & \langle \boldsymbol{\zeta} \mathbf{v}, \mathbf{u}_D - \mathbf{u}_h \rangle_{\Gamma_D} + \int_{\Omega} \left(\nabla\mathbf{u}_h - \frac{1}{\mu(\phi_h)}\boldsymbol{\sigma}_h^d \right) : \boldsymbol{\zeta} \\ & - \kappa_2 \int_{\Omega} (\mathbf{f}\phi_h - (\mathbf{K}^{-1}\mathbf{u}_h - \mathbf{div}\boldsymbol{\sigma}_h)) \cdot \mathbf{div}\boldsymbol{\zeta} \quad \forall \boldsymbol{\zeta} \in \mathbb{H}_N(\mathbf{div}, \Omega). \end{aligned} \tag{3.11}$$

3.2.2. A preliminary estimate for the concentration error

In contrast with [3, Section 3.2.2], in Lemma 3.3 below we establish an estimate for $\|\phi - \phi_h\|_{1,\Omega}$, whose proof, employing the ellipticity of the bilinear form $A_{\phi,\mathbf{u}}$ [2, eq. (3.13)], is provided later on in the Appendix. The reason for using the aforementioned ellipticity is due to fact that the Gâteaux derivative of the nonlinear operator induced by the form $A_{\mathbf{u}}$ (cf. (2.7)) is not elliptic as it was in [3], and hence we can not apply [3, Lemma 3.4] to derive the corresponding preliminary bound. In light of the above, we now set the following constants

$$\begin{aligned} \tilde{C} &:= \frac{1}{\alpha}, \quad C_3 := L_{\vartheta} C_{\delta} \tilde{C}_{\delta} \tilde{C}_{\zeta}(r), \quad C_4 := \tilde{C} (L_f + C_3 \gamma_2 |\Omega|^{1/2}), \quad C_5 := \tilde{C} C_3, \\ C_6 &:= 2\tilde{C}, \quad C_7 := r c(\Omega) \tilde{C} C_1, \quad C_8 := r c(\Omega) \tilde{C} C_2, \quad C_9 := r c(\Omega) \tilde{C}, \end{aligned} \tag{3.12}$$

where $\tilde{C}_{\zeta}(r)$, C_{δ} , \tilde{C}_{δ} and \tilde{C} are the constants provided by [2, eq. (3.24)], [2, Lemma 3.7, Theorem 3.10], and Lemma 3.2, respectively.

Lemma 3.3. Assume that the data \mathbf{k} , g , ϑ , \mathbf{u}_D , and \mathbf{f} are sufficiently small so that there holds

$$C_4 |\mathbf{k}| + C_5 \|g\|_{\delta,\Omega} + C_6 \vartheta_2 + C_7 \|\mathbf{u}_D\|_{1/2+\delta,\Gamma_D} + C_8 \|\mathbf{f}\|_{\infty,\Omega} < \frac{1}{2}. \tag{3.13}$$

Then, there exists $\hat{C} > 0$, depending on \tilde{C} and C_9 (cf. (3.12)), such that

$$\|\phi - \phi_h\|_{1,\Omega} \leq \hat{C} \left\{ \theta_0 + \|E_h\|_{\mathbb{H}_N(\mathbf{div},\Omega)'} + \|\tilde{E}_h\|_{H^1_{\Gamma_D}(\Omega)'} \right\}, \tag{3.14}$$

where θ_0 and E_h are given in the statement of Lemma 3.2 and (3.9), respectively, and $\tilde{E}_h \in H^1_{\Gamma_D}(\Omega)'$ is defined for each $\psi \in H^1_{\Gamma_D}(\Omega)$ by

$$\tilde{E}_h(\psi) := \int_{\Omega} (g - \beta \phi_h) \psi - \int_{\Omega} \left\{ \vartheta(\phi_h) \nabla \phi_h - \phi_h \mathbf{u}_h - f_{bk}(\phi_h) \mathbf{k} \right\} \cdot \nabla \psi. \tag{3.15}$$

In addition, there holds

$$\tilde{E}_h(\psi_h) = 0 \quad \forall \psi_h \in H^{\phi}_h. \tag{3.16}$$

We observe here that the upper bound in the assumption (3.13) could have been taken as any constant in $(0, 1)$. We have chosen $\frac{1}{2}$ for simplicity and also in order to minimise the resulting constant \hat{C} in (3.14). Furthermore, it is important to remark, according to (3.16), that for each $\psi \in H^1_{\Gamma_D}(\Omega)$ there holds $\tilde{E}_h(\psi) = \tilde{E}_h(\psi - \psi_h) \quad \forall \psi_h \in H^{\phi}_h$, and therefore $\|\tilde{E}_h\|_{H^1_{\Gamma_D}(\Omega)'}$ will be estimated below (see Subsection 3.2.3) by employing the foregoing expression with a suitable choice of $\psi_h \in H^{\phi}_h$.

3.2.3. A preliminary estimate for the total error

We now combine the inequalities provided by Lemmas 3.2 and 3.3 to derive a first estimate for the total error $\|\phi - \phi_h\|_{1,\Omega} + \|(\sigma, \mathbf{u}) - (\sigma_h, \mathbf{u}_h)\|_H$. To this end, we now introduce the constants

$$C(\mathbf{u}_D, \mathbf{f}) := \hat{C} \left\{ C_1 \|\mathbf{u}_D\|_{1/2+\varepsilon,\Gamma_D} + C_2 \|\mathbf{f}\|_{\infty,\Omega} + 1 \right\} \quad \text{and} \quad c(\mathbf{u}_D, \mathbf{f}) := \bar{C} + C(\mathbf{u}_D, \mathbf{f}),$$

where \bar{C} and \hat{C} are provided by Lemmas 3.2 and 3.3, respectively, and C_1 and C_2 are given by (3.6).

Theorem 3.4. Assume that

$$C_4 |\mathbf{k}| + C_5 \|g\|_{\delta,\Omega} + C_6 \vartheta_2 + C_7 \|\mathbf{u}_D\|_{1/2+\delta,\Gamma_D} + C_8 \|\mathbf{f}\|_{\infty,\Omega} < \frac{1}{2}.$$

Then there holds

$$\|\phi - \phi_h\|_{1,\Omega} + \|(\sigma, \mathbf{u}) - (\sigma_h, \mathbf{u}_h)\|_H \leq C(\mathbf{u}_D, \mathbf{f}) \|\tilde{E}_h\|_{H^1_{\Gamma_D}(\Omega)'} + c(\mathbf{u}_D, \mathbf{f}) \left\{ \theta_0 + \|E_h\|_{\mathbb{H}_N(\mathbf{div},\Omega)'} \right\}. \tag{3.17}$$

Proof. The estimate (3.17) is obtained by replacing the upper bound for $\|\phi - \phi_h\|_{1,\Omega}$, given by (3.14), into the second term on the right-hand side of (3.8), and then adding the result to the right-hand side of (3.14). \square

Having established the upper bound (3.17), and in order to obtain an explicit estimate for the total error, we turn to the derivation of suitable upper bounds for $\|\tilde{E}_h\|_{H^1_{\Gamma_D}(\Omega)'}$ and $\|E_h\|_{\mathbb{H}_N(\mathbf{div},\Omega)'}$.

3.2.4. Upper bounds for $\|\tilde{E}_h\|_{\mathbf{H}_{\Gamma_D}^1(\Omega)'}'$ and $\|E_h\|_{\mathbb{H}_N(\mathbf{div}, \Omega)'}'$

We begin by recalling the Clément interpolation operator $\mathcal{I}_h : \mathbf{H}^1(\Omega) \rightarrow X_h$ (cf. [19]), where

$$X_h := \{v_h \in C(\bar{\Omega}) : v_h|_T \in \mathbf{P}_1(T) \quad \forall T \in \mathcal{T}_h\},$$

and which satisfies the following local approximation properties of \mathcal{I}_h (for a proof, see [19]).

Lemma 3.5. *There exist constants $c_1, c_2 > 0$, independent of h , such that for all $v \in \mathbf{H}^1(\Omega)$ there hold*

$$\|v - \mathcal{I}_h(v)\|_{0,T} \leq c_1 h_T \|v\|_{1,\Delta(T)} \quad \forall T \in \mathcal{T}_h,$$

and

$$\|v - \mathcal{I}_h(v)\|_{0,e} \leq c_2 h_e^{1/2} \|v\|_{1,\Delta(e)} \quad \forall e \in \mathcal{E}_h,$$

where $\Delta(T)$ and $\Delta(e)$ are the union of all elements intersecting with T and e , respectively.

We now recall the definition of the concentration flux

$$\tilde{\sigma}_h := \vartheta(\phi_h) \nabla \phi_h - \phi_h \mathbf{u}_h - f_{bk}(\phi_h) \mathbf{k}. \tag{3.18}$$

Then, the following lemma provides an upper bound for $\|\tilde{E}_h\|_{\mathbf{H}_{\Gamma_D}^1(\Omega)'}'$.

Lemma 3.6. *Let $\tilde{\eta}^2 := \sum_{T \in \mathcal{T}_h} \tilde{\eta}_T^2$, where for each $T \in \mathcal{T}_h$ we set*

$$\tilde{\eta}_T^2 := h_T^2 \|g - (\beta \phi_h - \mathbf{div} \tilde{\sigma}_h)\|_{0,T}^2 + \sum_{e \in \mathcal{E}_h(T) \cap \mathcal{E}_h(\Omega)} h_e \|\llbracket \tilde{\sigma}_h \cdot \mathbf{v}_e \rrbracket\|_{0,e}^2 + \sum_{e \in \mathcal{E}_h(T) \cap \mathcal{E}_h(\Gamma_N)} h_e \|\tilde{\sigma}_h \cdot \mathbf{v}\|_{0,e}^2.$$

Then there exists $c > 0$, independent of h , such that

$$\|\tilde{E}_h\|_{\mathbf{H}_{\Gamma_D}^1(\Omega)'}' \leq c \tilde{\eta}.$$

Proof. It corresponds to a slight modification in the proof of [3, Lemma 3.8]. \square

Our next goal is to provide an upper bound for $\|E_h\|_{\mathbb{H}_N(\mathbf{div}, \Omega)'}'$ (cf. (3.9)), which, being less straightforward than Lemma 3.6, requires several preliminary results. To this end, we start by introducing the space

$$\mathbf{H}_{\Gamma_N}^1(\Omega) := \left\{ \boldsymbol{\varphi} \in \mathbf{H}^1(\Omega) : \boldsymbol{\varphi} = \mathbf{0} \text{ on } \Gamma_N \right\},$$

and establishing a suitable Helmholtz decomposition of our space $\mathbb{H}_N(\mathbf{div}, \Omega)$.

Lemma 3.7. *Assume that Ω is a connected domain and that Γ_N is contained in the boundary of a convex extension of Ω . Then, for each $\boldsymbol{\zeta} \in \mathbb{H}_N(\mathbf{div}, \Omega)$, there exist $\boldsymbol{\tau} \in \mathbf{H}^1(\Omega)$ and $\boldsymbol{\chi} \in \mathbf{H}_{\Gamma_N}^1(\Omega)$ such that*

$$\boldsymbol{\zeta} = \boldsymbol{\tau} + \mathbf{curl}(\boldsymbol{\chi}) \text{ in } \Omega, \tag{3.19}$$

and

$$\|\boldsymbol{\tau}\|_{1,\Omega} + \|\boldsymbol{\chi}\|_{1,\Omega} \leq C \|\boldsymbol{\zeta}\|_{\mathbf{div},\Omega}, \tag{3.20}$$

with a positive constant C independent of $\boldsymbol{\zeta}$.

Proof. See [3, Lemma 3.9]. \square

We continue our analysis by introducing the following finite element subspace of $\mathbf{H}_{\Gamma_N}(\Omega)$

$$\mathbf{X}_{h,N} := \left\{ \boldsymbol{\varphi}_h \in \mathbf{C}(\bar{\Omega}) : \boldsymbol{\varphi}_h|_T \in \mathbf{P}_1(T) \quad \forall T \in \mathcal{T}_h, \quad \boldsymbol{\varphi}_h = \mathbf{0} \text{ on } \Gamma_N \right\},$$

and considering, analogously as before, the Clément interpolation operator $\mathcal{I}_{h,N} : \mathbf{H}_{\Gamma_N}(\Omega) \rightarrow \mathbf{X}_{h,N}$. In addition, we let $\Pi_h : \mathbf{H}^1(\Omega) \rightarrow \mathbb{H}_h^\sigma$ be the Raviart–Thomas interpolation operator (see [12], [34]), which, according to its characterisation properties (see e.g. [24, Section 3.4.1]), verifies

$$\mathbf{div}(\Pi_h(\bar{\boldsymbol{\tau}})) = \mathcal{P}_h(\mathbf{div}\bar{\boldsymbol{\tau}}) \quad \forall \bar{\boldsymbol{\tau}} \in \mathbb{H}^1(\Omega), \tag{3.21}$$

where $\mathcal{P}_h : \mathbf{L}^2(\Omega) \rightarrow \mathbf{Q}_h$ is the $\mathbf{L}^2(\Omega)$ -orthogonal projector and

$$\mathbf{Q}_h := \{ \mathbf{v} \in \mathbf{L}^2(\Omega) : \mathbf{v}|_T \in \mathbf{P}_k(T) \quad \forall T \in \mathcal{T}_h \}.$$

Further approximation properties of Π_h are summarised as follows (see [24, Lemmas 3.16 and 3.18]).

Lemma 3.8. *There exist $c_3, c_4 > 0$, independent of h , such that for all $\bar{\boldsymbol{\tau}} \in \mathbb{H}^1(\Omega)$ there holds*

$$\|\bar{\boldsymbol{\tau}} - \Pi_h(\bar{\boldsymbol{\tau}})\|_{0,T} \leq c_3 h_T \|\bar{\boldsymbol{\tau}}\|_{1,T} \quad \forall T \in \mathcal{T}_h,$$

and

$$\|(\bar{\boldsymbol{\tau}} - \Pi_h(\bar{\boldsymbol{\tau}})) \mathbf{v}\|_{0,e} \leq c_4 h_e^{1/2} \|\bar{\boldsymbol{\tau}}\|_{1,T_e} \quad \forall e \in \mathcal{E}_h(\Omega) \cup \mathcal{E}_h(\Gamma_D),$$

where T_e is a triangle of \mathcal{T}_h containing the edge e on its boundary.

Next, given $\boldsymbol{\zeta} \in \mathbb{H}_N(\mathbf{div}, \Omega)$ and its Helmholtz decomposition (3.19), we define $\boldsymbol{\chi}_h := \mathcal{I}_{h,N}(\boldsymbol{\zeta})$, and set

$$\boldsymbol{\zeta}_h := \Pi_h(\boldsymbol{\tau}) + \mathbf{curl}(\boldsymbol{\chi}_h) \in \mathbb{H}_h^\sigma \tag{3.22}$$

as its associated discrete Helmholtz decomposition. Then, from (3.19) and (3.22), it follows that

$$\boldsymbol{\zeta} - \boldsymbol{\zeta}_h = \boldsymbol{\tau} - \Pi_h(\boldsymbol{\tau}) + \mathbf{curl}(\boldsymbol{\chi} - \boldsymbol{\chi}_h).$$

Therefore, according to (3.9) and (3.10), we deduce that

$$E_h(\boldsymbol{\zeta}) = E_h(\boldsymbol{\zeta} - \boldsymbol{\zeta}_h) = E_h(\boldsymbol{\tau} - \Pi_h(\boldsymbol{\tau})) + E_h(\mathbf{curl}(\boldsymbol{\chi} - \boldsymbol{\chi}_h)). \tag{3.23}$$

Notice from (3.23) that, in order to estimate $\|E_h\|_{\mathbb{H}_N(\mathbf{div}, \Omega)}$, it only remains to bound $|E_h(\boldsymbol{\tau} - \Pi_h(\boldsymbol{\tau}))|$ and $|E_h(\mathbf{curl}(\boldsymbol{\chi} - \boldsymbol{\chi}_h))|$ in terms of a multiple of $\|\boldsymbol{\zeta}\|_{\mathbf{div}, \Omega}$, which is done in the rest of the present Section 3.2.4. To this end, we now recall from [21] the following integration by parts formula on the boundary.

Lemma 3.9. *There holds*

$$\langle \mathbf{curl} \boldsymbol{\chi} \mathbf{v}, \boldsymbol{\phi} \rangle = - \langle \frac{d\boldsymbol{\phi}}{ds}, \boldsymbol{\chi} \rangle \quad \forall \boldsymbol{\chi}, \boldsymbol{\phi} \in \mathbf{H}^1(\Omega). \tag{3.24}$$

Proof. It follows from suitable applications of the Green formulae provided in [30, Chapter I, eq. (2.17) and Theorem 2.11]. \square

Lemma 3.10. *Let $\theta_1^2 := \sum_{T \in \mathcal{T}_h} \theta_{1,T}^2$, where for each $T \in \mathcal{T}_h$ we set*

$$\begin{aligned} \theta_{1,T}^2 := & h_T^2 \left\| \mathbf{curl} \left\{ \frac{1}{\mu(\phi_h)} \boldsymbol{\sigma}_h^{\mathbf{d}} \right\} \right\|_{0,T}^2 + \sum_{e \in \mathcal{E}_h(T) \cap \mathcal{E}_h(\Omega)} h_e \left\| \left[\frac{1}{\mu(\phi_h)} \boldsymbol{\sigma}_h^{\mathbf{d}} \mathbf{s} \right] \right\|_{0,e}^2 \\ & + \sum_{e \in \mathcal{E}_h(T) \cap \mathcal{E}_h(\Gamma_D)} h_e \left\| \frac{d\mathbf{u}_D}{ds} - \frac{1}{\mu(\phi_h)} \boldsymbol{\sigma}_h^{\mathbf{d}} \mathbf{s} \right\|_{0,e}^2. \end{aligned}$$

Then there exists $c > 0$, independent of h , such that

$$|E_h(\mathbf{curl}(\boldsymbol{\chi} - \boldsymbol{\chi}_h))| \leq c \theta_1 \|\boldsymbol{\zeta}\|_{\mathbf{div}, \Omega}. \tag{3.25}$$

Proof. See [3, Lemma 3.11]. \square

Lemma 3.11. *Let $\theta_2^2 := \sum_{T \in \mathcal{T}_h} \theta_{2,T}^2$, where for each $T \in \mathcal{T}_h$ we set*

$$\theta_{2,T}^2 := h_T^2 \left\| \nabla \mathbf{u}_h - \frac{1}{\mu(\phi_h)} \boldsymbol{\sigma}_h^{\mathbf{d}} \right\|_{0,T}^2 + \|\mathbf{f} \phi_h - (\mathbf{K}^{-1} \mathbf{u}_h - \mathbf{div} \boldsymbol{\sigma}_h)\|_{0,T}^2 + \sum_{e \in \mathcal{E}_h(T) \cap \mathcal{E}_h(\Gamma_D)} h_e \|\mathbf{u}_D - \mathbf{u}_h\|_{0,e}^2.$$

Then there exists $c > 0$, independent of h , such that

$$|E_h(\boldsymbol{\tau} - \Pi_h(\boldsymbol{\tau}))| \leq c \theta_2 \|\boldsymbol{\zeta}\|_{\mathbf{div}, \Omega}. \tag{3.26}$$

Proof. Using the alternative definition of the functional E_h (cf. (3.11)), applying the identity (3.21), and denoting by \mathcal{I} a generic identity operator, we find that

$$E_h(\boldsymbol{\tau} - \Pi_h(\boldsymbol{\tau})) = \langle (\boldsymbol{\tau} - \Pi_h(\boldsymbol{\tau})) \mathbf{v}, \mathbf{u}_D - \mathbf{u}_h \rangle_{\Gamma_D} + \int_{\Omega} \left(\nabla \mathbf{u}_h - \frac{1}{\mu(\phi_h)} \boldsymbol{\sigma}_h^d \right) : (\boldsymbol{\tau} - \Pi_h(\boldsymbol{\tau})) - \kappa_2 \int_{\Omega} (\mathbf{f} \phi_h - (\mathbf{K}^{-1} \mathbf{u}_h - \mathbf{div} \boldsymbol{\sigma}_h)) \cdot (\mathcal{I} - \mathcal{P}_h)(\mathbf{div} \boldsymbol{\tau}). \tag{3.27}$$

Next, the first two terms on the right-hand side of (3.27) are simply bounded by applying the Cauchy–Schwarz in $\mathbf{L}^2(\Gamma_D)$ and $\mathbb{L}^2(\Omega)$, and then employing the approximation properties of Π_h provided by Lemma 3.8. In turn, for the corresponding third term, it suffices to see, thanks to the Cauchy–Schwarz inequality and the stability estimate (3.20), that

$$\left| \int_{\Omega} (\mathbf{f} \phi_h - (\mathbf{K}^{-1} \mathbf{u}_h - \mathbf{div} \boldsymbol{\sigma}_h)) \cdot (\mathcal{I} - \mathcal{P}_h)(\mathbf{div} \boldsymbol{\tau}) \right| \leq \| \mathbf{f} \phi_h - (\mathbf{K}^{-1} \mathbf{u}_h - \mathbf{div} \boldsymbol{\sigma}_h) \|_{0,\Omega} \| \mathbf{div} \boldsymbol{\tau} \|_{0,\Omega} \leq \| \mathbf{f} \phi_h - (\mathbf{K}^{-1} \mathbf{u}_h - \mathbf{div} \boldsymbol{\sigma}_h) \|_{0,\Omega} \| \boldsymbol{\zeta} \|_{\mathbf{div},\Omega},$$

which ends the proof. \square

By virtue of Lemmas 3.10 and 3.11 we deduce the following upper bound for $\|E_h\|_{\mathbb{H}_N(\mathbf{div},\Omega)'}.$

Lemma 3.12. *There exists $c > 0$, independent of h , such that*

$$\|E_h\|_{\mathbb{H}_N(\mathbf{div},\Omega)'} \leq c \{ \boldsymbol{\theta}_1 + \boldsymbol{\theta}_2 \}.$$

Proof. It follows straightforwardly from (3.23) and the upper bounds (3.25) and (3.26). \square

At this point we remark that the terms $h_T^2 \| \nabla \mathbf{u}_h - \frac{1}{\mu(\phi_h)} \boldsymbol{\sigma}_h^d \|_{0,T}^2$ and $h_e \| \mathbf{u}_D - \mathbf{u}_h \|_{0,e}^2$, which appear in the definition of $\theta_{2,T}^2$ (cf. Lemma 3.11), are dominated by $\| \nabla \mathbf{u}_h - \frac{1}{\mu(\phi_h)} \boldsymbol{\sigma}_h^d \|_{0,T}^2$ and $\| \mathbf{u}_D - \mathbf{u}_h \|_{0,e}^2$, respectively, which form part of $\theta_{0,T}^2$ (cf. (3.7)). Therefore, the reliability estimate (3.5) (cf. Theorem 3.1) is a direct consequence of Theorem 3.4, the definition of θ_0 (cf. Lemma 3.2), and Lemmas 3.6, 3.10, 3.11, and 3.12.

We close this section by mentioning that the assumption (3.4) on the data $\vartheta, \mathbf{k}, \mathbf{g}, \mathbf{u}_D$, and \mathbf{f} , which, as shown throughout the foregoing analysis, is a key estimate to derive (3.5), is, unfortunately, unverifiable in practice. In fact, while the data are certainly known in advance, the constants C_4, C_5, C_6, C_7, C_8 involved in that condition (cf. (3.12)), which in turn are expressed in terms of the previous constants C_1 and C_2 (cf. (3.6)), depend all on boundedness and regularity constants of operators, as well as on parameters, some of which are not explicitly calculable, and hence it is not possible to check whether (3.4) is indeed satisfied or not. This is, however, a quite common fact arising in the analysis of many nonlinear problems, and only in very particular cases (usually related to simple geometries of the domain) it could eventually be circumvented.

3.3. Efficiency

The main result of this section is stated as follows.

Theorem 3.13. *Assume that $\nabla \phi \in \mathbf{L}^4(\Omega)$. Then, there exists a constant $\bar{C}_{\text{eff}} > 0$, which depends only on parameters, $\| \mathbf{K}^{-1} \|_{\infty}, |\mathbf{k}|, \| \mathbf{u}_D \|_{1/2,\Gamma_D}, \| \mathbf{f} \|_{\infty,\Omega}, \| \nabla \phi \|_{\mathbf{L}^4(\Omega)}$ and other constants, all them independent of h , such that*

$$\bar{C}_{\text{eff}} \boldsymbol{\theta} \leq \| \phi - \phi_h \|_{1,\Omega} + \| \mathbf{u} - \mathbf{u}_h \|_{1,\Omega} + \| \mathbf{div}(\boldsymbol{\sigma} - \boldsymbol{\sigma}_h) \|_{0,\Omega} + \left\| \frac{1}{\mu(\phi)} \boldsymbol{\sigma}^d - \frac{1}{\mu(\phi_h)} \boldsymbol{\sigma}_h^d \right\|_{0,\Omega} + \text{h.o.t.} \tag{3.28}$$

where h.o.t. stands for one or several terms of higher order. Moreover, under the assumption that $\boldsymbol{\sigma} \in \mathbb{L}^4(\Omega)$, there exists a constant $C_{\text{eff}} > 0$, which depends only on parameters, $\| \mathbf{K}^{-1} \|_{\infty}, |\mathbf{k}|, \| \mathbf{u}_D \|_{1/2,\Gamma_D}, \| \mathbf{f} \|_{\infty,\Omega}, \| \boldsymbol{\sigma} \|_{\mathbb{L}^4(\Omega)}, \| \nabla \phi \|_{\mathbf{L}^4(\Omega)}$ and other constants, all them independent of h , such that

$$C_{\text{eff}} \boldsymbol{\theta} \leq \| \phi - \phi_h \|_{1,\Omega} + \| (\boldsymbol{\sigma}, \mathbf{u}) - (\boldsymbol{\sigma}_h, \mathbf{u}_h) \|_H + \text{h.o.t.} \tag{3.29}$$

In the subsequent analysis we assume for simplicity, but without loss of generality, that the nonlinear functions μ, ϑ , and f_{bk} are such that $\frac{1}{\mu(\phi_h)}, \vartheta(\phi_h), f_{bk}(\phi_h)$, and hence $\tilde{\boldsymbol{\sigma}}_h$ as well, are all piecewise polynomials. In addition, we

assume that the data \mathbf{u}_D and g are piecewise polynomials. Otherwise, and if μ^{-1} , ϑ , f_{bk} , \mathbf{u}_D , and g are sufficiently smooth, higher order terms given by the errors arising from suitable polynomial approximations of these expressions and functions would appear in (3.28) and (3.29) (cf. Theorem 3.13), which explains the eventual h.o.t. in these expressions. In this regard, and similarly as observed in [3], we remark that (3.28) constitutes a *quasi-efficiency* estimate for the global residual error estimator θ (cf. (3.3)). Indeed, the fact that the expression appearing on the right-hand side of (3.28) is not exactly the error, but part of it plus the nonlinear term given by $\|\frac{1}{\mu(\phi)}\sigma^d - \frac{1}{\mu(\phi_h)}\sigma_h^d\|_{0,\Omega}$, explains the *quasi-efficiency* concept employed here. Nevertheless, we show at the end of this section that, under the assumption that $\sigma \in \mathbb{L}^4(\Omega)$, the latter can be bounded by $\|\sigma - \sigma_h\|_{0,\Omega} + \|\phi - \phi_h\|_{1,\Omega}$, thus yielding the efficiency estimate given by (3.29).

In order to prove (3.28) and (3.29), in the rest of this section we derive suitable upper bounds for the ten terms defining the local error indicator θ_T^2 (cf. (3.2)). We begin by observing, thanks to the fact that $\mathbf{f}\phi = \mathbf{K}^{-1}\mathbf{u} - \mathbf{div}\sigma$ in Ω , that there holds

$$\begin{aligned} \|\mathbf{f}\phi_h - (\mathbf{K}^{-1}\mathbf{u}_h - \mathbf{div}\sigma_h)\|_{0,T}^2 &\leq 2\|\mathbf{f}\|_{\infty,\Omega}^2\|\phi - \phi_h\|_{0,T}^2 \\ &+ 4\|\mathbf{K}^{-1}\|_{\infty}^2\|\mathbf{u} - \mathbf{u}_h\|_{0,T}^2 + 4\|\mathbf{div}(\sigma - \sigma_h)\|_{0,T}^2. \end{aligned} \tag{3.30}$$

On the other hand, using that $\nabla\mathbf{u} = \frac{1}{\mu(\phi)}\sigma^d$ in Ω , $\mathbf{u} = \mathbf{u}_D$ on Γ_D , and proceeding as in [3, Section 3.3], we deduce that

$$\left\|\nabla\mathbf{u}_h - \frac{1}{\mu(\phi_h)}\sigma_h^d\right\|_{0,T}^2 \leq 2\|\nabla\mathbf{u} - \nabla\mathbf{u}_h\|_{0,T}^2 + 2\left\|\frac{1}{\mu(\phi)}\sigma^d - \frac{1}{\mu(\phi_h)}\sigma_h^d\right\|_{0,T}^2 \tag{3.31}$$

and

$$\sum_{e \in \mathcal{E}_h(\Gamma_D)} \|\mathbf{u}_D - \mathbf{u}_h\|_{0,e}^2 \leq c_0^2\|\mathbf{u} - \mathbf{u}_h\|_{1,\Omega}^2, \tag{3.32}$$

where c_0 is the norm of the trace operator in $\mathbf{H}^1(\Omega)$.

The efficiency estimates for the remaining six terms given in (3.3), are provided next. To this end, we proceed as in [17] and [18] (see also [23]), and apply the localisation technique (see [41]) based on triangle-bubble and edge-bubble functions, together with extension operators, and inverse inequalities. In what follows, given $e \in \mathcal{E}_h(\Omega)$, ω_e denotes the union of the two triangles in \mathcal{T}_h having e as an edge, whereas for each $e \in \mathcal{E}_h(\Gamma_D) \cup \mathcal{E}_h(\Gamma_N)$ we let T_e be the triangle of \mathcal{T}_h having e as an edge.

In turn, the following lemma, whose proof make use of the estimates for the bubble functions and the inverse inequality, will be required for the terms involving the **curl** operator and the tangential jumps across the edges of \mathcal{T}_h .

Lemma 3.14. *Let $\rho_h \in \mathbb{L}^2(\Omega)$ be a piecewise polynomial of degree $k \geq 0$ on each $T \in \mathcal{T}_h$. In addition, let $\rho \in \mathbb{L}^2(\Omega)$ be such that $\mathbf{curl}(\rho) = 0$ on each $T \in \mathcal{T}_h$. Then, there exist $c, \tilde{c} > 0$, independent of h , such that*

$$\|\mathbf{curl}(\rho_h)\|_{0,T} \leq ch_T^{-1}\|\rho - \rho_h\|_{0,T} \quad \forall T \in \mathcal{T}_h$$

and

$$\|\llbracket \rho_h \mathbf{s}_e \rrbracket\|_{0,e} \leq \tilde{c}h_e^{-1/2}\|\rho - \rho_h\|_{0,\omega_e} \quad \forall e \in \mathcal{E}_h(\Omega).$$

Proof. For the first estimate we refer to [17, Lemma 4.3], whereas the second one follows from a slight modification of the proof of [17, Lemma 4.4]. Further details are omitted. \square

We now provide upper bounds for three other terms defining θ_T^2 .

Lemma 3.15. *There exist constants $\tilde{c}_1, \tilde{c}_2, \tilde{c}_3 > 0$, independent of h such that*

$$\begin{aligned} h_T^2 \left\| \mathbf{curl} \left\{ \frac{1}{\mu(\phi_h)} \sigma_h^d \right\} \right\|_{0,T}^2 &\leq \tilde{c}_1 \left\| \frac{1}{\mu(\phi)} \sigma^d - \frac{1}{\mu(\phi_h)} \sigma_h^d \right\|_{0,T}^2 & \forall T \in \mathcal{T}_h, \\ h_e \left\| \left[\left[\frac{1}{\mu(\phi_h)} \sigma_h^d \mathbf{s} \right] \right] \right\|_{0,e}^2 &\leq \tilde{c}_2 \left\| \frac{1}{\mu(\phi)} \sigma^d - \frac{1}{\mu(\phi_h)} \sigma_h^d \right\|_{0,\omega_e}^2 & \forall e \in \mathcal{E}_h(\Omega), \\ h_e \left\| \frac{d\mathbf{u}_D}{ds} - \frac{1}{\mu(\phi_h)} \sigma_h^d \mathbf{s} \right\|_{0,e}^2 &\leq \tilde{c}_3 \left\| \frac{1}{\mu(\phi)} \sigma^d - \frac{1}{\mu(\phi_h)} \sigma_h^d \right\|_{0,T_e}^2 & \forall e \in \mathcal{E}_h(\Gamma_D). \end{aligned}$$

Proof. For the first two estimates it suffices to apply Lemma 3.14 to $\rho_h := \frac{1}{\mu(\phi_h)}\sigma_h^d$ and $\rho := \frac{1}{\mu(\phi)}\sigma^d = \nabla\mathbf{u}$, whereas for the third one we proceed similarly as in the proof of [28, Lemma 4.15], by replacing \mathbf{g} , Γ , and $\frac{1}{\mu}\sigma_h^d$ in [28] by \mathbf{u}_D , Γ_D , and $\frac{1}{\mu(\phi_h)}\sigma_h^d$, respectively. \square

We now aim to provide upper bounds for the three terms completing the definition of the local error indicator θ_T^2 (cf. (3.2)). This requires, however, the preliminary result given by the following a priori estimate for the error $\|\tilde{\sigma} - \tilde{\sigma}_h\|_{0,T}^2$.

Lemma 3.16. *There exists $C > 0$, depending on ϑ_2 , L_f (cf. (2.3), (2.4)), and $|\mathbf{k}|$, such that*

$$\|\tilde{\sigma} - \tilde{\sigma}_h\|_{0,T}^2 \leq C \left\{ \|\phi - \phi_h\|_{1,T}^2 + \|\mathbf{u}(\phi - \phi_h)\|_{0,T}^2 + \|\phi_h(\mathbf{u} - \mathbf{u}_h)\|_{0,T}^2 + \|(\vartheta(\phi) - \vartheta(\phi_h))\nabla\phi\|_{0,T}^2 \right\}. \tag{3.33}$$

Proof. Employing the definitions of $\tilde{\sigma}$ (cf. (2.1)) and $\tilde{\sigma}_h$ (cf. (3.18)), applying the triangle inequality, and using the Lipschitz continuity assumption on f_{bk} (cf. (2.4)), but restricted to each $T \in \mathcal{T}_h$ instead of Ω , we obtain that

$$\begin{aligned} \|\tilde{\sigma} - \tilde{\sigma}_h\|_{0,T}^2 \leq 2 \left\{ \|\vartheta(\phi)\nabla\phi - \vartheta(\phi_h)\nabla\phi_h\|_{0,T}^2 + 2L_f^2|\mathbf{k}|^2\|\phi - \phi_h\|_{0,T}^2 \right. \\ \left. + 4\|\mathbf{u}(\phi - \phi_h)\|_{0,T}^2 + 4\|\phi_h(\mathbf{u} - \mathbf{u}_h)\|_{0,T}^2 \right\}. \end{aligned} \tag{3.34}$$

In turn, applying Cauchy–Schwarz’s inequality and the upper bound for ϑ (cf. (3.13)), we deduce that

$$\|\vartheta(\phi)\nabla\phi - \vartheta(\phi_h)\nabla\phi_h\|_{0,T}^2 \leq 2\|(\vartheta(\phi) - \vartheta(\phi_h))\nabla\phi\|_{0,T}^2 + 2\vartheta_2^2\|\nabla\phi - \nabla\phi_h\|_{0,T}^2. \tag{3.35}$$

In this way, (3.34) and (3.35) imply (3.33), which finalises the proof. \square

We consider important to remark here that, due to the dependence on ϕ (instead of $|\nabla\phi|$ as in [3]) of the diffusivity ϑ , the first term of our nonlinear operator $A_{\mathbf{u}}$ is not necessarily Lipschitz-continuous (as it was the case for the corresponding nonlinear operator in [3, eq. (2.11)]) and hence, in contrast with [3, Lemma 3.19], now the term $\|(\vartheta(\phi) - \vartheta(\phi_h))\nabla\phi\|_{0,T}^2$ appears in the estimate (3.33) of Lemma 3.16. The treatment of such additional term will be postponed to Lemma 3.18.

We now establish the aforementioned efficiency estimates.

Lemma 3.17. *There exist $\tilde{c}_4, \tilde{c}_5, \tilde{c}_6 > 0$, which depend only on ϑ_2 , L_f , β (cf. (2.3), (2.4), (2.1)), $|\mathbf{k}|$, and other constants, all them independent of h , such that*

$$\begin{aligned} h_T^2\|g - (\beta\phi_h - \operatorname{div}\tilde{\sigma}_h)\|_{0,T}^2 \leq \tilde{c}_4 \left\{ \|\phi - \phi_h\|_{1,T}^2 + \|\mathbf{u}(\phi - \phi_h)\|_{0,T}^2 \right. \\ \left. + \|\phi_h(\mathbf{u} - \mathbf{u}_h)\|_{0,T}^2 + \|(\vartheta(\phi) - \vartheta(\phi_h))\nabla\phi\|_{0,T}^2 + h_T^2\|\phi - \phi_h\|_{0,T}^2 \right\} \quad \forall T \in \mathcal{T}_h, \end{aligned} \tag{3.36}$$

$$\begin{aligned} h_e\|[\tilde{\sigma}_h \cdot \mathbf{v}_e]\|_{0,e}^2 \leq \tilde{c}_5 \sum_{T \subseteq \omega_e} \left\{ \|\phi - \phi_h\|_{1,T}^2 + \|\mathbf{u}(\phi - \phi_h)\|_{0,T}^2 + \|\phi_h(\mathbf{u} - \mathbf{u}_h)\|_{0,T}^2 \right. \\ \left. + \|(\vartheta(\phi) - \vartheta(\phi_h))\nabla\phi\|_{0,T}^2 + h_T^2\|\phi - \phi_h\|_{0,T}^2 \right\} \quad \forall e \in \mathcal{E}_h(\Omega), \end{aligned} \tag{3.37}$$

and

$$\begin{aligned} h_e\|\tilde{\sigma}_h \cdot \mathbf{v}\|_{0,e}^2 \leq \tilde{c}_6 \left\{ \|\phi - \phi_h\|_{1,T_e}^2 + \|\mathbf{u}(\phi - \phi_h)\|_{0,T_e}^2 + \|\phi_h(\mathbf{u} - \mathbf{u}_h)\|_{0,T_e}^2 \right. \\ \left. + \|(\vartheta(\phi) - \vartheta(\phi_h))\nabla\phi\|_{0,T_e}^2 + h_{T_e}^2\|\phi - \phi_h\|_{0,T_e}^2 \right\} \quad \forall e \in \mathcal{E}_h(\Gamma_N). \end{aligned} \tag{3.38}$$

Proof. The estimate (3.36) follows from an adaptation of the proof of [3, Lemma 3.22] by using the properties of the bubble functions, the integration by parts procedure, the Cauchy–Schwarz inequality, and the inverse estimate. We omit further details. In turn, (3.37) and (3.38) were established in [3, Lemmas 3.21 and 3.22]. \square

In order to complete the proof of global efficiency given by (3.28), it only remains to estimate properly the three terms: $\|\mathbf{u}(\phi - \phi_h)\|_{0,T}^2$, $\|\phi_h(\mathbf{u} - \mathbf{u}_h)\|_{0,T}^2$ and $\|(\vartheta(\phi) - \vartheta(\phi_h))\nabla\phi\|_{0,T}^2$, appearing in the upper bounds provided by the last four lemmas, which is indeed the purpose of the following lemma, and whose proof is provided in the Appendix.

Lemma 3.18. *There exist positive constants \tilde{c}_7, \tilde{c}_8 , independent of h , such that*

$$\sum_{T \in \mathcal{T}_h} \|\mathbf{u}(\phi - \phi_h)\|_{0,T}^2 \leq \tilde{c}_7\|\phi - \phi_h\|_{1,\Omega}^2 \quad \text{and} \quad \sum_{T \in \mathcal{T}_h} \|\phi_h(\mathbf{u} - \mathbf{u}_h)\|_{0,T}^2 \leq \tilde{c}_8\|\mathbf{u} - \mathbf{u}_h\|_{1,\Omega}^2, \tag{3.39}$$

where \tilde{c}_7 depends on $\|\mathbf{u}_D\|_{1/2,\Gamma_D}$, $\|\mathbf{f}\|_{\infty,\Omega}$ and r (cf. (3.1)), and \tilde{c}_8 depends on r . In addition, assuming $\nabla\phi \in L^4(\Omega)$, there exists a positive constant \tilde{c}_9 , independent of h , such that

$$\sum_{T \in \mathcal{T}_h} \|(\vartheta(\phi) - \vartheta(\phi_h))\nabla\phi\|_{0,T}^2 \leq \tilde{c}_9 \|\phi - \phi_h\|_{1,\Omega}^2, \tag{3.40}$$

where \tilde{c}_9 depends on L_ϑ (cf. (2.4)) and $\|\nabla\phi\|_{L^4(\Omega)}$.

By virtue of the estimates (3.30), (3.31), (3.32), Lemmas 3.15, and 3.17, and the final estimates given by (3.39) and (3.40), we deduce (3.28). Finally, assuming now that $\sigma \in \mathbb{L}^4(\Omega)$ and proceeding as at the end of the proof of [3, Theorem 3.13], we find that

$$\left\| \frac{1}{\mu(\phi)}\sigma^d - \frac{1}{\mu(\phi_h)}\sigma_h^d \right\|_{0,\Omega} \leq C \left\{ \|\sigma - \sigma_h\|_{0,\Omega} + \|\phi - \phi_h\|_{1,\Omega} \right\}, \tag{3.41}$$

where C is a positive constant, independent of h , that depends only on μ_1 (cf. (2.3)), L_μ (cf. (2.4)) and $\|\sigma\|_{\mathbb{L}^4(\Omega)}$. In this way, combining (3.41) and (3.28), we arrive at (3.29), which completes the proof of Theorem 3.13.

4. A second residual-based a posteriori error estimator

In this section we describe another *a posteriori* error estimator for our augmented mixed-primal finite element scheme (2.10), with the same discrete spaces introduced in the Section 2.3. In turn, the reliability of our new estimator can be proved without resorting to Helmholtz decompositions. More precisely, this second estimator arises simply employing the alternative definition of the functional E_h (cf. (3.11)) and bounding $\|E_h\|_{\mathbb{H}_N(\text{div},\Omega)}$ in the preliminary estimate for the total error given by (3.17) (cf. Theorem 3.4). Then, with the same notations and discrete spaces introduced in Sections 2 and 3, we now set for each $T \in \mathcal{T}_h$ the local error indicator

$$\begin{aligned} \tilde{\theta}_T^2 := & \|\mathbf{f}\phi_h - (\mathbf{K}^{-1}\mathbf{u}_h - \text{div}\sigma_h)\|_{0,T}^2 + \left\| \nabla\mathbf{u}_h - \frac{1}{\mu(\phi_h)}\sigma_h^d \right\|_{0,T}^2 + h_T^2 \|g - (\beta\phi_h - \text{div}\tilde{\sigma}_h)\|_{0,T}^2 \\ & + \sum_{e \in \mathcal{E}_h(T) \cap \mathcal{E}_h(\Omega)} h_e \|\llbracket \tilde{\sigma}_h \cdot \mathbf{v}_e \rrbracket\|_{0,e}^2 + \sum_{e \in \mathcal{E}_h(T) \cap \mathcal{E}_h(\Gamma_N)} h_e \|\tilde{\sigma}_h \cdot \mathbf{v}\|_{0,e}^2 + \sum_{e \in \mathcal{E}_h(T) \cap \mathcal{E}_h(\Gamma_D)} \|\mathbf{u}_D - \mathbf{u}_h\|_{0,e}^2, \end{aligned} \tag{4.1}$$

and define the following global residual error estimator

$$\tilde{\theta}^2 := \sum_{T \in \mathcal{T}_h} \tilde{\theta}_T^2 + \|\mathbf{u}_D - \mathbf{u}_h\|_{1/2,\Gamma_D}^2. \tag{4.2}$$

Then, it is not difficult to establish *quasi-local* reliability and efficiency for the estimator $\tilde{\theta}$. The name *quasi-local* refers here to the fact that the last term defining $\tilde{\theta}$ can not be decomposed into local quantities associated to each triangle $T \in \mathcal{T}_h$, unless it is either conveniently bounded or previously modified, as we explain in what follows. In fact, in order to use the indicator $\tilde{\theta}$ (cf. (4.2)) in an adaptive algorithm that solves (2.10), we need to estimate the expression $\|\mathbf{u}_D - \mathbf{u}_h\|_{1/2,\Gamma_D}^2$ through local terms. To this end, as well as in [3], we now employ an interpolation argument and replace the aforementioned expression by a suitable upper bound, which yields a reliable and fully local *a posteriori* error estimate.

Theorem 4.1. Assume that the data \mathbf{k} , g , ϑ , \mathbf{u}_D , and \mathbf{f} are sufficiently small so that there holds

$$C_4 \|\mathbf{k}\| + C_5 \|g\|_{\delta,\Omega} + C_6 \vartheta_2 + C_7 \|\mathbf{u}_D\|_{1/2+\delta,\Gamma_D} + C_8 \|\mathbf{f}\|_{\infty,\Omega} < \frac{1}{2},$$

where C_4, C_5, C_6, C_7 and C_8 are the constants given in (3.12). In turn, let $\hat{\theta}^2 := \sum_{T \in \mathcal{T}_h} \hat{\theta}_T^2$, where for each $T \in \mathcal{T}_h$ we set

$$\begin{aligned} \hat{\theta}_T^2 := & \|\mathbf{f}\phi_h - (\mathbf{K}^{-1}\mathbf{u}_h - \text{div}\sigma_h)\|_{0,T}^2 + \left\| \nabla\mathbf{u}_h - \frac{1}{\mu(\phi_h)}\sigma_h^d \right\|_{0,T}^2 + h_T^2 \|g - (\beta\phi_h - \text{div}\tilde{\sigma}_h)\|_{0,T}^2 \\ & + \sum_{e \in \mathcal{E}_h(T) \cap \mathcal{E}_h(\Omega)} h_e \|\llbracket \tilde{\sigma}_h \cdot \mathbf{v}_e \rrbracket\|_{0,e}^2 + \sum_{e \in \mathcal{E}_h(T) \cap \mathcal{E}_h(\Gamma_N)} h_e \|\tilde{\sigma}_h \cdot \mathbf{v}\|_{0,e}^2 + \sum_{e \in \mathcal{E}_h(T) \cap \mathcal{E}_h(\Gamma_D)} \|\mathbf{u}_D - \mathbf{u}_h\|_{1,e}^2. \end{aligned}$$

Then, there exists a constant $\hat{C}_{\text{rel}} > 0$, which depends only on parameters, $\|\mathbf{u}_D\|_{1/2+\delta,\Gamma_D}$, $\|\mathbf{f}\|_{\infty,\Omega}$ and other constants, all them independent of h , such that

$$\|\phi - \phi_h\|_{1,\Omega}^2 + \|(\sigma, \mathbf{u}) - (\sigma_h, \mathbf{u}_h)\|_H^2 \leq \hat{C}_{\text{rel}} \hat{\theta}^2.$$

Proof. The proof reduces to bound the term $\|\mathbf{u}_D - \mathbf{u}_h\|_{1/2, \Gamma_D}$. To this end, it suffices to apply the fact that $H^{1/2}(\Gamma_D)$ is the interpolation space with index 1/2 between $H^1(\Gamma_D)$ and $L^2(\Gamma_D)$, and proceed as in [3, Theorem 4.3]. \square

5. Residual-based a posteriori error estimators: the 3D case

In this section we extend the results from Sections 3 and 4 to the three-dimensional version of (2.10). Analogously, as in Section 3, given a tetrahedron $T \in \mathcal{T}_h$, we let $\mathcal{E}_h(T)$ be the set of its faces, and let \mathcal{E}_h be the set of all faces of the triangulation \mathcal{T}_h . Then, we write $\mathcal{E}_h = \mathcal{E}_h(\Omega) \cup \mathcal{E}_h(\Gamma)$, where $\mathcal{E}_h(\Omega) := \{e \in \mathcal{E}_h : e \subseteq \Omega\}$ and $\mathcal{E}_h(\Gamma) := \{e \in \mathcal{E}_h : e \subseteq \Gamma\}$. Also, for each face $e \in \mathcal{E}_h$ we fix a unit normal \mathbf{v}_e to e , so that given $\boldsymbol{\tau} \in \mathbb{L}^2(\Omega)$ such that $\boldsymbol{\tau}|_T \in \mathbb{C}(T)$ on each $T \in \mathcal{T}_h$, and given $e \in \mathcal{E}_h(\Omega)$, we let $\llbracket \boldsymbol{\tau} \times \mathbf{v}_e \rrbracket$ be the corresponding jump of the tangential traces across e , that is $\llbracket \boldsymbol{\tau} \times \mathbf{v}_e \rrbracket := (\boldsymbol{\tau}|_T - \boldsymbol{\tau}|_{T'})|_e \times \mathbf{v}_e$, where T and T' are the elements of \mathcal{T}_h having e as a common face. In what follows, when no confusion arises, we simply write \mathbf{v} instead of \mathbf{v}_e .

Now, we recall that the curl of a 3D vector $\mathbf{v} := (v_1, v_2, v_3)$ is the 3D vector

$$\text{curl}(\mathbf{v}) = \nabla \times \mathbf{v} := \left(\frac{\partial v_3}{\partial x_2} - \frac{\partial v_2}{\partial x_3}, \frac{\partial v_1}{\partial x_3} - \frac{\partial v_3}{\partial x_1}, \frac{\partial v_2}{\partial x_1} - \frac{\partial v_1}{\partial x_2} \right),$$

and that, given a tensor function $\boldsymbol{\tau} := (\tau_{ij})_{3 \times 3}$, the operator **curl** denotes curl acting along each row of $\boldsymbol{\tau}$, and $\boldsymbol{\tau} \times \mathbf{v}$ is a tensor whose rows are the tangential components of each row of $\boldsymbol{\tau}$, that is,

$$\mathbf{curl}(\boldsymbol{\tau}) := \begin{pmatrix} \text{curl}(\tau_{11}, \tau_{12}, \tau_{13}) \\ \text{curl}(\tau_{21}, \tau_{22}, \tau_{23}) \\ \text{curl}(\tau_{31}, \tau_{32}, \tau_{33}) \end{pmatrix}, \quad \text{and} \quad \boldsymbol{\tau} \times \mathbf{v} := \begin{pmatrix} (\tau_{11}, \tau_{12}, \tau_{13}) \times \mathbf{v} \\ (\tau_{21}, \tau_{22}, \tau_{23}) \times \mathbf{v} \\ (\tau_{31}, \tau_{32}, \tau_{33}) \times \mathbf{v} \end{pmatrix}.$$

We now set for each $T \in \mathcal{T}_h$ the local *a posteriori* error indicator θ_T^2 as follows

$$\begin{aligned} \theta_T^2 := & \|\mathbf{f}\phi_h - (\mathbf{K}^{-1}\mathbf{u}_h - \mathbf{div}\boldsymbol{\sigma}_h)\|_{0,T}^2 + \left\| \nabla\mathbf{u}_h - \frac{1}{\mu(\phi_h)}\boldsymbol{\sigma}_h^d \right\|_{0,T}^2 + h_T^2 \|g - (\beta\phi_h - \mathbf{div}\tilde{\boldsymbol{\sigma}}_h)\|_{0,T}^2 \\ & + h_T^2 \left\| \mathbf{curl} \left\{ \frac{1}{\mu(\phi_h)}\boldsymbol{\sigma}_h^d \right\} \right\|_{0,T}^2 + \sum_{e \in \mathcal{E}_h(T) \cap \mathcal{E}_h(\Omega)} h_e \left\| \llbracket \frac{1}{\mu(\phi_h)}\boldsymbol{\sigma}_h^d \times \mathbf{v} \rrbracket \right\|_{0,e}^2 \\ & + \sum_{e \in \mathcal{E}_h(T) \cap \mathcal{E}_h(\Omega)} h_e \|\llbracket \tilde{\boldsymbol{\sigma}}_h \cdot \mathbf{v}_e \rrbracket\|_{0,e}^2 + \sum_{e \in \mathcal{E}_h(T) \cap \mathcal{E}_h(\Gamma_N)} h_e \|\tilde{\boldsymbol{\sigma}}_h \cdot \mathbf{v}\|_{0,e}^2 \\ & + \sum_{e \in \mathcal{E}_h(T) \cap \mathcal{E}_h(\Gamma_D)} \|\mathbf{u}_D - \mathbf{u}_h\|_{0,e}^2 + \sum_{e \in \mathcal{E}_h(T) \cap \mathcal{E}_h(\Gamma_D)} h_e \left\| \nabla\mathbf{u}_D \times \mathbf{v} - \frac{1}{\mu(\phi_h)}\boldsymbol{\sigma}_h^d \times \mathbf{v} \right\|_{0,e}^2, \end{aligned} \tag{5.1}$$

whereas $\tilde{\theta}_T^2$ stays exactly as in (4.1). In this way, the corresponding global *a posteriori* error estimators are defined as (3.3) and (4.2), that is

$$\boldsymbol{\theta}^2 := \sum_{T \in \mathcal{T}_h} \theta_T^2 \quad \text{and} \quad \tilde{\boldsymbol{\theta}}^2 := \sum_{T \in \mathcal{T}_h} \tilde{\theta}_T^2 + \|\mathbf{u}_D - \mathbf{u}_h\|_{1/2, \Gamma_D}^2.$$

We now establish the analogue of Theorem 3.1.

Theorem 5.1 (Reliability of $\boldsymbol{\theta}$). Assume that Ω is a connected domain and that Γ_N is the boundary of a convex extension of Ω . In addition, assume that the data $\mathbf{k}, g, \vartheta, \mathbf{u}_D$, and \mathbf{f} are sufficiently small so that there holds

$$C_4 \|\mathbf{k}\| + C_5 \|g\|_{\delta, \Omega} + C_6 \vartheta_2 + C_7 \|\mathbf{u}_D\|_{1/2+\delta, \Gamma_D} + C_8 \|\mathbf{f}\|_{\infty, \Omega} < \frac{1}{2},$$

where C_4, C_5, C_6, C_7 and C_8 are the constants given below in (3.12). Then, there exists a constant $C_{\text{rel}} > 0$, which depends only on parameters, $\|\mathbf{u}_D\|_{1/2+\delta, \Gamma_D}, \|\mathbf{f}\|_{\infty, \Omega}$, and other constants, all them independent of h , such that

$$\|\phi - \phi_h\|_{1, \Omega} + \|(\boldsymbol{\sigma}, \mathbf{u}) - (\boldsymbol{\sigma}_h, \mathbf{u}_h)\|_H \leq C_{\text{rel}} \boldsymbol{\theta}.$$

The proof of Theorem 5.1 follows from a very similar analysis to the Section 3.2, except in a few points to be described throughout the following discussion. Indeed, we first need to use a 3D version of the stable Helmholtz decomposition, provided by Lemma 3.7, which was established recently in [25, Theorem 3.2]. We remark that the proof of [25, Theorem 3.2] makes use of several estimates available in [6] and combines similar arguments to those from the proofs of [25, Theorem 3.1]

and [3, Lemma 3.9]. Then, the associated discrete Helmholtz decomposition and the functional E_h are set and rewritten exactly as in (3.22) and (3.23), respectively. Secondly, in order to derive the upper bound to $\|E_h\|_{\mathbb{H}_N(\mathbf{div}, \Omega)^\prime}$, we need to employ the 3D analogue of the integration by parts formula on the boundary given by (3.24) (cf. Lemma 3.9). In fact, by employing the identities from [30, Chapter I, eq. (2.17) and Theorem 2.11], we find that in the 3D case, there holds

$$\langle \mathbf{curl} \chi, \mathbf{v}, \phi \rangle = -\langle \nabla \phi \times \mathbf{v}, \chi \rangle \quad \forall \chi \in \mathbb{H}^1(\Omega), \quad \forall \phi \in \mathbb{H}^1(\Omega). \tag{5.2}$$

On the other hand, the integration by parts formula on each tetrahedron $T \in \mathcal{T}_h$, which is employed in the proof of the 3D analogue of Lemma 3.10 (see also [3, Lemma 3.11]), becomes (cf. [30, Chapter I, Theorem 2.11])

$$\int_T \mathbf{curl} \tau : \chi - \int_T \tau : \mathbf{curl} \chi = \langle \tau \times \mathbf{v}, \chi \rangle_{\partial T} \quad \forall \tau \in \mathbb{H}(\mathbf{curl}; \Omega), \quad \forall \chi \in \mathbb{H}^1(\Omega), \tag{5.3}$$

where $\langle \cdot, \cdot \rangle_{\partial T}$ is the duality pairing between $\mathbb{H}^{-1/2}(T)$ and $\mathbb{H}^{1/2}(T)$, and, as usual, $\mathbb{H}(\mathbf{curl}; \Omega)$ corresponds to the space of tensors in $\mathbb{L}^2(\Omega)$ whose \mathbf{curl} belongs to $\mathbb{L}^2(\Omega)$. Notice that the identities (5.2) and (5.3) explain the appearing of the expressions $\frac{1}{\mu(\phi_h)} \sigma_h^d \times \mathbf{v}$ and $\nabla \mathbf{u}_D \times \mathbf{v} - \frac{1}{\mu(\phi_h)} \sigma_h^d \times \mathbf{v}$ in the 3D definition of θ (cf. (5.1)). Then, we have the following result.

Theorem 5.2 (Reliability of $\tilde{\theta}$). Assume that the data $\mathbf{k}, \mathbf{g}, \vartheta, \mathbf{u}_D$, and \mathbf{f} are sufficiently small so that there holds

$$C_4 \|\mathbf{k}\| + C_5 \|\mathbf{g}\|_{\delta, \Omega} + C_6 \vartheta_2 + C_7 \|\mathbf{u}_D\|_{1/2+\delta, \Gamma_D} + C_8 \|\mathbf{f}\|_{\infty, \Omega} < \frac{1}{2},$$

where C_4, C_5, C_6, C_7 and C_8 are the constants given in (3.12). Then, there exists a constant $\tilde{C}_{\text{re1}} > 0$, which depends only on $\|\mathbf{u}_D\|_{1/2+\delta, \Gamma_D}, \|\mathbf{f}\|_{\infty, \Omega}$ and other constants, all them independent of h , such that

$$\|\phi - \phi_h\|_{1, \Omega}^2 + \|(\sigma, \mathbf{u}) - (\sigma_h, \mathbf{u}_h)\|_H^2 \leq \tilde{C}_{\text{re1}} \tilde{\theta}^2.$$

We end this section by remarking that the efficiency of the estimators θ and $\tilde{\theta}$ follows as in Sections 3.3 and 4. In particular, we remark that the 3D version of estimates provided in Lemmas 3.14 and 3.15 can be derived from [27, Lemmas 4.9, 4.10, 4.11 and 4.13].

6. Numerical tests

This section serves to illustrate the properties of the estimators introduced in Sections 3–5. Fixed point iterations were used for the linearisation of the coupled mixed-primal scheme, and a residual tolerance of $1e-7$ was prescribed for the termination of the Picard algorithm. All linear solves are performed with the unsymmetric multifrontal direct solver MUMPS. In addition, all tests in this Section use a classical adaptive mesh refinement procedure based on the equi-distribution of the error indicators, where the diameter of each element in the new adapted mesh (contained in a generic element K on the initial coarse mesh) is proportional to the diameter of the initial element times the ratio $\frac{\bar{\eta}_h}{\eta_K}$, where $\bar{\eta}_h$ is the mean value of a given indicator η over the initial mesh (cf. [40]).

6.1. Example 1: accuracy assessment

Our first example focuses on the case where, under uniform mesh refinement, the convergence rates are affected by the singularities of the exact solutions. A non-convex domain $\Omega := (0, 1)^2 \setminus [0, \frac{1}{2}]^2$ is considered, and its boundary $\partial\Omega$ is split into $\Gamma_N := [1, 0] \times \{0\}$ and $\Gamma_D := \partial\Omega \setminus \Gamma_N$. We construct a sequence of nested unstructured triangulations, where measured errors and experimental convergence rates will be computed as usual

$$e(\sigma) = \|\sigma - \sigma_h\|_{\mathbf{div}, \Omega}, \quad e(\phi) = \|\phi - \phi_h\|_{1, \Omega}, \quad e(\mathbf{u}) = \|\mathbf{u} - \mathbf{u}_h\|_{1, \Omega}, \quad r(\cdot) = -2 \log(e(\cdot)/\hat{e}(\cdot)) [\log(N/\hat{N})]^{-1},$$

with e and \hat{e} denoting errors produced on two consecutive meshes representing N and \hat{N} degrees of freedom, respectively. In addition, the total error, the modified error suggested by (3.28), and the effectivity and quasi-effectivity indexes associated to a given global estimator η are defined, respectively, as

$$e = \{[e(\sigma)]^2 + [e(\mathbf{u})]^2 + [e(\phi)]^2\}^{1/2}, \quad \text{eff}(\eta) = \frac{e}{\eta},$$

$$m = \left\{ [e(\mathbf{u})]^2 + [e(\phi)]^2 + \|\mathbf{div} \sigma - \mathbf{div} \sigma_h\|_{0, \Omega}^2 + \left\| \frac{\sigma^d}{\mu(\phi)} - \frac{\sigma_h^d}{\mu(\phi_h)} \right\|_{0, \Omega}^2 \right\}^{1/2}, \quad \text{qeff}(\eta) = \frac{m}{\eta}.$$

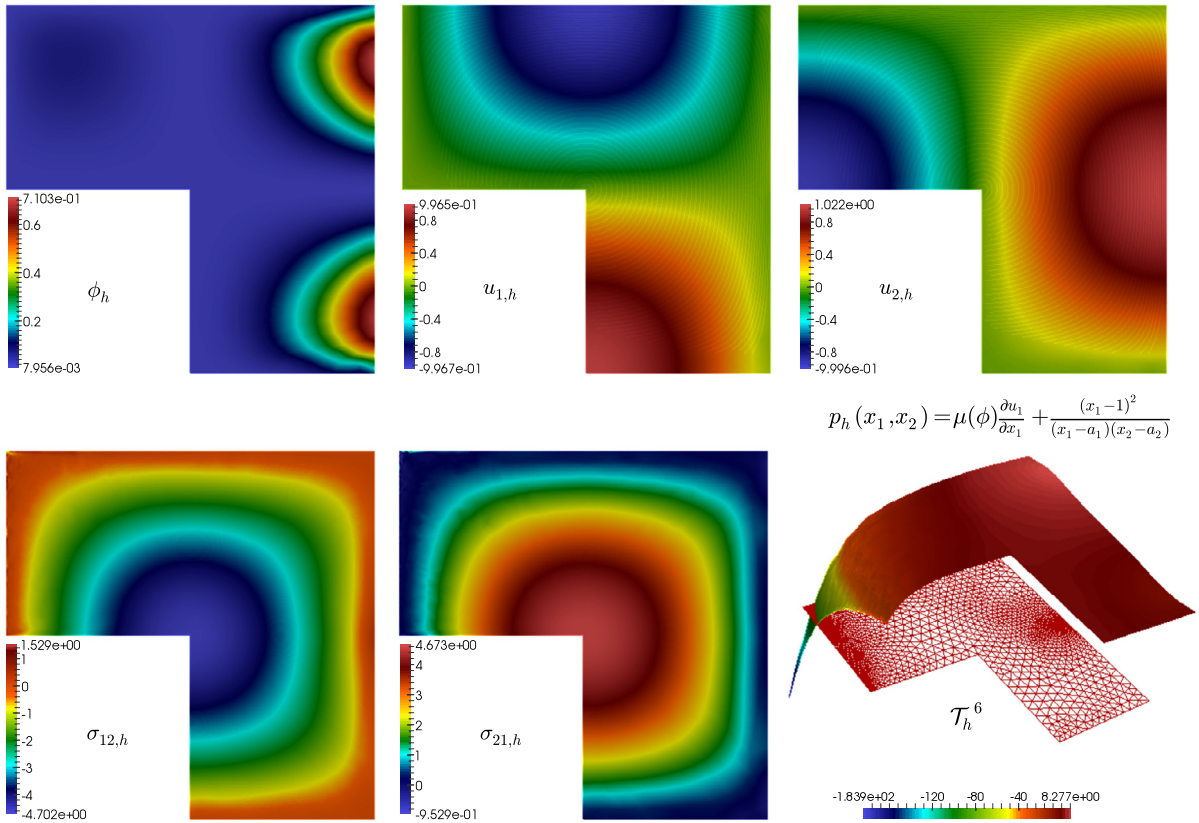


Fig. 6.1. Example 1. Approximate solutions obtained with the lowest order method, after six steps of adaptive mesh refinement following the second indicator $\tilde{\theta}$. Concentration, velocity components, and stress secondary components, and postprocessed pressure and adapted mesh emphasising the clustering of points near (a_1, a_2) . (For interpretation of the colours in the figure(s), the reader is referred to the web version of this article.)

An exact solution to (2.1) is given as follows

$$\begin{aligned} \phi(x_1, x_2) &= mx_1x_2(1 - x_2)(x_1 - 1/2)^2(x_2 - 1/2)^2 + b, \\ \mathbf{u}(x_1, x_2) &= \begin{pmatrix} \sin(\pi x_1) \cos(\pi x_2) \\ -\cos(\pi x_1) \sin(\pi x_2) \end{pmatrix}, \quad \sigma(x_1, x_2) = \mu(\phi)\mathbf{u} - \left[\mu(\phi) \frac{\partial \mathbf{u}_1}{\partial x_1} + \frac{(x_1 - 1)^2}{(x_2 - a_1)(x_2 - a_2)} \right] \mathbb{I}, \end{aligned} \tag{6.1}$$

where $\mathbf{K}^{-1} = K^{-1}\mathbb{I}$, $\mathbf{k} = (0, -1)^t$, $\mu(\phi) = (1 - a\phi)^{-2}$, $f_{bk}(\phi) = a\phi(1 - a\phi)^2$, $\vartheta(\phi) = \phi + (1 - a\phi)^2$, and the source terms are

$$\mathbf{f}(x_1, x_2) = \phi^{-1}(K^{-1}\mathbf{u} - \mathbf{div}\sigma), \quad g(x_1, x_2) = \beta\phi - \mathbf{div}(\vartheta(\phi)\nabla\phi) + \mathbf{u} \cdot \nabla\phi + f'_{bk}(\phi)\mathbf{k} \cdot \nabla\phi.$$

Notice that the only difference with respect to (2.1) is a non-homogeneous concentration flux $\tilde{\sigma} \cdot \mathbf{v} = s$ imposed on Γ_N , where s is manufactured according to (6.1). Therefore, the relevant term in the *a posteriori* error estimators will be replaced by

$$\sum_{e \in \mathcal{E}_h(T) \cap \mathcal{E}_h(\Gamma_N)} h_e \|\tilde{\sigma}_h \cdot \mathbf{v} - s\|_{0,e}^2,$$

whose estimation from below and above follows in a straightforward way. The model parameters specifying (6.1) correspond to $m = 20$, $b = 0.008$, $a = 0.35$, $K = 0.01$, $\beta = 0.35$, and $a_1 = -0.05$, $a_2 = 1.1$. Notice that the pressure defining the isotropic part of the stress in (6.1) exhibits a singularity near the upper right corner of the domain, at (a_1, a_2) (see the bottom-right panel of Fig. 6.1). As a consequence, optimal convergence for the stress is no longer evidenced under uniform mesh refinement (see first rows of Table 1). In turn, if an adaptive mesh refinement step (employing the residual error indicators θ and $\tilde{\theta}$) is applied, optimal convergence can be restored, as shown in the last two blocks of Table 1. Approximated solutions obtained after six adaptation steps are collected in Fig. 6.1, and a few adapted meshes produced using the two indicators are depicted in Fig. 6.2. It is observed that the agglomeration of points follows the regions of high concentration gradients occurring near Γ_N , as well as the sharp pressure profile localised at (a_1, a_2) .

Table 1

Example 1. Convergence history, Picard iteration count, error e and quasi-error m , effectivity and quasi-effectivity indexes for the approximation of the coupled Brinkman-transport problem, under quasi-uniform, and adaptive refinement according to the indicators introduced in Sections 3 and 4.

D.o.f.	h	$e(\sigma)$	$r(\sigma)$	$e(\mathbf{u})$	$r(\mathbf{u})$	$e(\phi)$	$r(\phi)$	i_p	e	m	$\text{eff}(\theta)$	$\text{qeff}(\theta)$	$\text{eff}(\tilde{\theta})$	$\text{qeff}(\tilde{\theta})$
Augmented $\mathbf{RT}_0 - \mathbf{P}_1 - \mathbf{P}_1$ scheme with quasi-uniform refinement														
105	0.53	14.05	–	3.40	–	1.43	–	12	17.01	18.42	1.11	1.10	1.10	1.10
192	0.49	22.54	0.44	8.81	2.90	1.35	0.80	16	29.56	31.53	0.55	0.55	0.55	0.55
492	0.30	13.93	0.97	3.36	1.95	0.87	0.88	14	16.93	17.77	1.07	1.07	1.07	1.07
1488	0.16	7.45	1.01	0.82	2.27	0.47	0.98	12	7.45	7.44	0.92	0.92	0.92	0.92
4902	0.09	4.40	0.88	0.28	1.77	0.26	0.98	13	6.05	5.98	0.96	0.96	0.96	0.95
17800	0.04	2.14	1.05	0.12	1.25	0.14	0.88	13	4.46	4.43	0.98	0.98	0.98	0.98
67800	0.02	1.15	1.14	0.05	1.36	0.07	1.33	14	2.48	2.46	1.00	1.00	0.99	0.99
Augmented $\mathbf{RT}_0 - \mathbf{P}_1 - \mathbf{P}_1$ scheme with adaptive refinement according to θ														
64	0.61	20.32	–	8.93	–	1.40	–	16	30.42	27.77	0.49	0.48	–	–
171	0.35	13.88	0.77	3.07	2.17	1.18	0.34	16	18.82	18.09	1.24	1.23	–	–
303	0.33	9.97	1.15	1.98	1.52	1.10	0.26	14	12.94	11.37	0.95	0.94	–	–
499	0.30	6.84	1.51	1.27	1.78	1.09	0.03	13	8.38	7.07	1.05	1.05	–	–
1014	0.21	3.90	1.58	0.78	1.35	0.85	0.69	13	6.06	5.83	1.17	1.17	–	–
3763	0.10	1.65	1.31	0.26	1.66	0.37	1.26	13	4.52	4.45	1.07	1.07	–	–
14690	0.05	0.78	1.09	0.11	1.27	0.17	1.07	13	2.81	2.79	1.03	1.03	–	–
Augmented $\mathbf{RT}_0 - \mathbf{P}_1 - \mathbf{P}_1$ scheme with adaptive refinement according to $\tilde{\theta}$														
64	0.61	20.32	–	8.93	–	1.40	–	16	30.42	29.77	–	–	0.49	0.47
171	0.35	13.88	0.77	3.07	2.17	1.18	0.34	16	18.82	18.09	–	–	1.24	1.23
303	0.33	9.96	1.15	1.97	1.54	1.10	0.26	14	12.66	11.29	–	–	0.95	0.94
535	0.28	7.11	1.18	1.41	1.18	1.08	0.04	13	8.14	8.61	–	–	1.06	1.05
1145	0.21	3.79	1.65	0.60	2.24	0.80	0.79	13	6.88	6.64	–	–	1.08	1.08
4270	0.10	1.69	1.22	0.24	1.35	0.38	1.11	13	4.94	4.88	–	–	1.05	1.05
16790	0.05	0.82	1.04	0.10	1.25	0.18	1.10	13	2.28	2.26	–	–	1.02	1.01

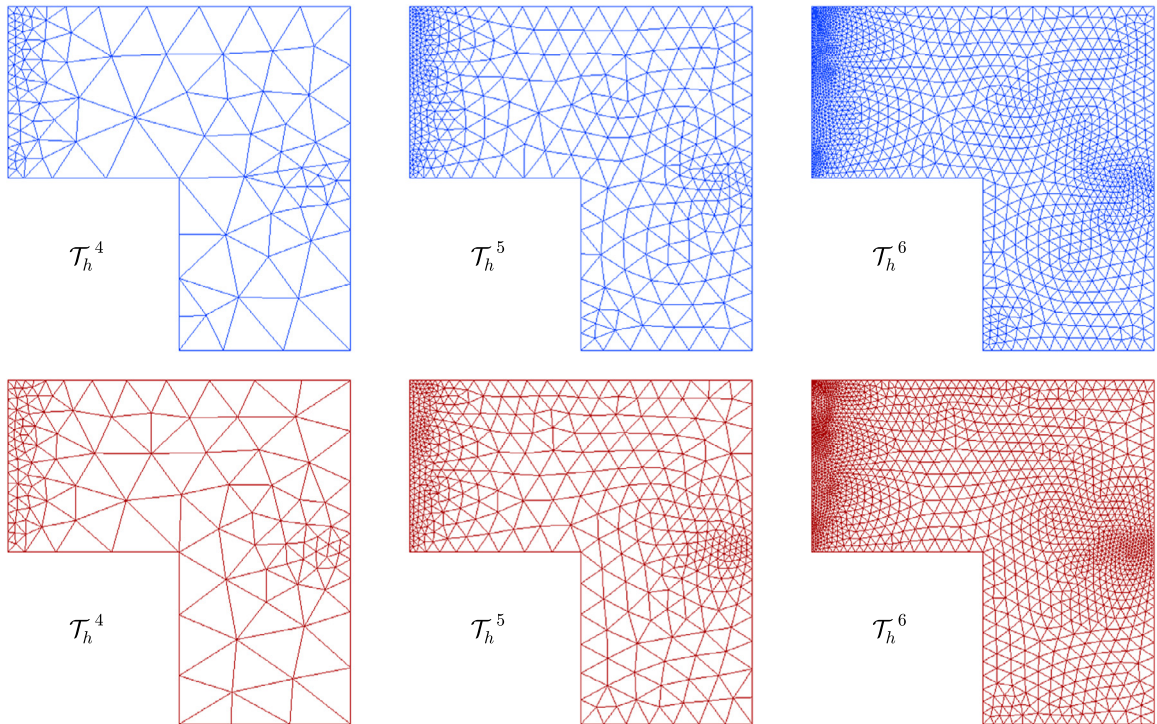


Fig. 6.2. Example 1. From left to right, three snapshots of successively refined meshes according to the indicators θ and $\tilde{\theta}$ (top and bottom panels, respectively).

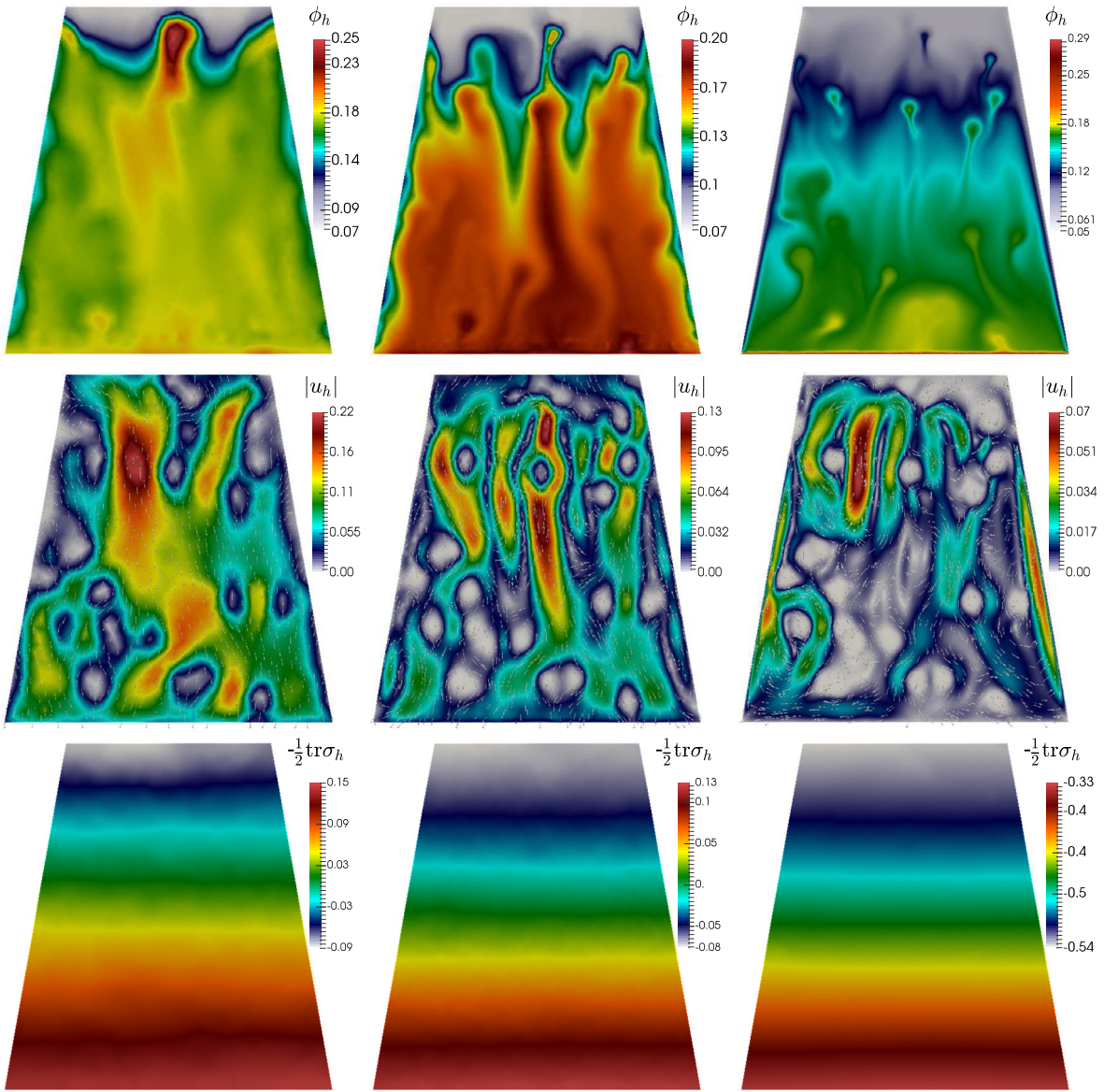


Fig. 6.3. Example 2. Approximate solutions at 3 (left), 6 (middle) and 12 (right) pseudo-time steps. A lowest order method and mesh adaptive refinement guided by (4.2) were used.

6.2. Example 2: sedimentation below downward-facing inclined walls

This test illustrates the properties of the second estimator (4.2) in a 2D setting, where we simulate the sedimentation of a mixture within an heterogeneous porous medium. The domain consists of an isosceles trapeze of height 3, maximal width 2.82, and walls having an angle of inclination of $4/9\pi$ with respect to the horizontal axis. The permeability of the medium is constant K_0 , except for 20 randomly placed spots (consisting of disks with radii $2.5e-3$) of much lower permeability K_1 . Viscosity, hindering sedimentation, and compaction coefficients (all concentration-dependent) are respectively specified as

$$\mu(\phi) = \mu_0(1 - \phi/\phi_{\max})^{-\eta_1}, \quad f_{\text{bk}}(\phi) = u_\infty\phi(1 - \phi/\phi_{\max})^{\eta_2}, \quad \vartheta(\phi) = \frac{\sigma_0\alpha}{\phi_c^\alpha \Delta\rho G} \phi^{\alpha-2} f_{\text{bk}} + u_\infty, \quad (6.2)$$

where the model parameters and remaining constants assume the values $\mu_0 = 2.5e-4$, $\sigma_0 = 5.5e-4$, $G = 9.81$, $\alpha = 5$, $\beta = 0.25$, $\eta = 2$, $\phi_c = 0.07$, $\phi_{\max} = 0.95$, $K_0 = 10$, $K_1 = 0.01$, $\mathbf{k} = (0, -1)^T$, $\mathbf{f} = (0, -1/2)^T$, $u_\infty = 2.5e-3$, $\Delta\rho = 1562$. From the physical bounds of the concentration we find $\mu_1 = \mu_0$ and $\mu_2 = 5\mu_1$, yielding the following stabilisation coefficients $\kappa_1 = 1/5\mu_0^2 = 5e-5$, $\alpha_K = 0.1$, $\delta = 4.88e-3$, $\kappa_2 = 2.38e-6$.

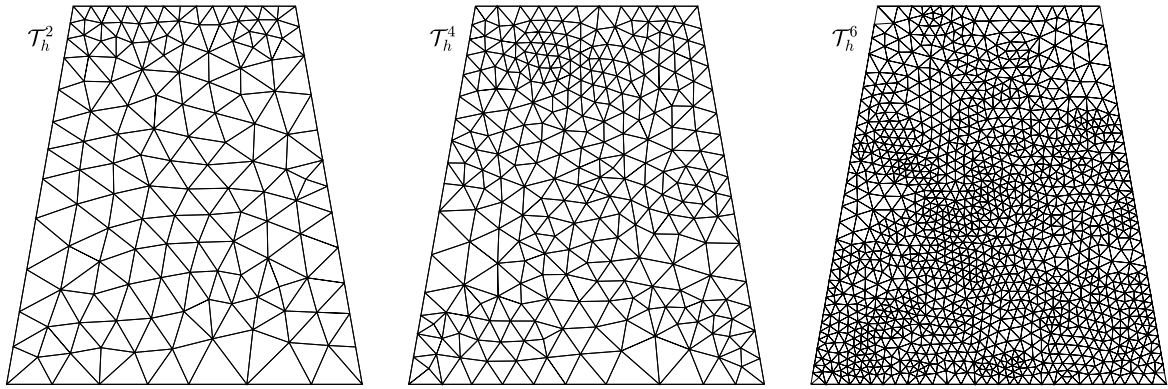


Fig. 6.4. Example 2. Adapted meshes at 2, 4, and 6 steps, generated following the second estimator (4.2).

Table 2

Example 2. Experimental convergence against a reference solution, number of fixed-point iterations, and quasi-effectivity indexes for the approximation of the sedimentation problem under inclined walls, using the *a posteriori* error indicator (4.2).

D.o.f.	h	$e(\sigma)$	$r(\sigma)$	$e(\mathbf{u})$	$r(\mathbf{u})$	$e(\phi)$	$r(\phi)$	i_P	$\text{qeff}(\tilde{\theta})$
Quasi-uniform refinement									
69	0.532	40.12	–	10.22	–	0.91	–	10	2.59
214	0.494	31.63	0.49	8.81	0.60	0.66	0.63	11	3.15
578	0.302	22.65	0.67	5.63	0.43	0.42	0.57	14	2.21
1341	0.168	15.80	0.45	3.55	0.27	0.27	0.83	11	5.29
5027	0.095	13.45	0.28	2.23	0.24	0.21	0.37	12	1.88
12538	0.048	9.46	0.55	2.02	0.15	0.17	0.24	13	6.47
Adaptive mesh refinement according to $\tilde{\theta}$									
69	0.532	40.12	–	10.22	–	0.91	–	10	2.59
122	0.253	25.29	0.81	4.63	1.30	0.39	1.32	8	2.63
315	0.131	13.41	0.90	2.12	1.38	0.16	1.19	9	2.61
1076	0.045	8.02	0.96	0.92	1.21	0.08	0.99	10	2.60
4577	0.012	4.19	1.10	0.47	1.03	0.03	1.18	9	2.59
10903	0.002	1.07	1.12	0.09	1.53	0.01	0.92	9	2.60

A pseudo time-advancing algorithm is employed to capture the transient nature of the phenomenon (this can be achieved by setting $g = \beta\phi^k$, where ϕ^k is the concentration distribution at the previous pseudo timestep). The initial guess for the concentration is a relatively high value $\phi = 0.75$ on the top of the domain and a random perturbation of amplitude 0.05 around $\phi = 0.15$. We assume that the vessel is open on the top and closed elsewhere on $\partial\Omega$, so that a clear fluid $\phi = \phi_c$ and zero normal stresses $\sigma \nu = \mathbf{0}$ are prescribed on top, whereas on the remainder of the boundary we set zero fluxes $\tilde{\sigma} \cdot \nu = 0$ and no-slip conditions $\mathbf{u} = \mathbf{0}$.

The adaptive algorithm applies mesh refinement according to the second *a posteriori* error indicator (4.2), and it is invoked at the end of each pseudo-time step. We point out that due to the roughness of the permeability for coarser meshes, a continuation technique is applied on the viscosity scaling μ_0 (using $\tilde{\mu}_0 = 8\mu_0$ as initial guess, and halving it until reaching μ_0). A set of snapshots of the numerical solution obtained after ten pseudo-time steps are displayed in Fig. 6.3. Apart from the main flow features expected in the pure-fluid case (acceleration of the deposition near the inclined walls, as discussed in [37] and simulated in [36,35]), we also observe tortuous concentration and velocity patterns produced by a combination of tight flow-transport coupling, the highly heterogeneous coefficients, and the random initial distribution. The velocity plots (second row) indicate that the flow tends to avoid the regions of low permeability, and recirculation zones are formed near the transition from clear to high-concentration mixture. In addition, the concentration plots (panels in the first row) suggest that solid particles remain attached to the low-permeability spots and reverse plumes are formed. We also show a sequence of refined meshes after two, four, and six steps (see Fig. 6.4), where it is seen that the *a posteriori* error indicator yields more refinement near the high gradients of concentration and the aforementioned recirculation zones. As these irregularities spread throughout large portions of the domain, a substantial gain in computational cost with respect to a uniformly refined mesh is not expected.

We also conduct an experimental error analysis, restricted to the solution of the problem after two pseudo timesteps, in order to corroborate the appropriateness of the scheme and the features of the *a posteriori* error estimators. Lacking a closed form for the exact solution of problem (2.1), we proceed to generate a highly refined mesh and regard the solution computed on this grid, using an augmented $\mathbf{RT}_1 - \mathbf{P}_2 - \mathbf{P}_2$ scheme, as a reference solution for error computation. Table 2 reports on the error history under both uniform and adaptive refinement. Rates are sub-optimal for the first case (particularly for the

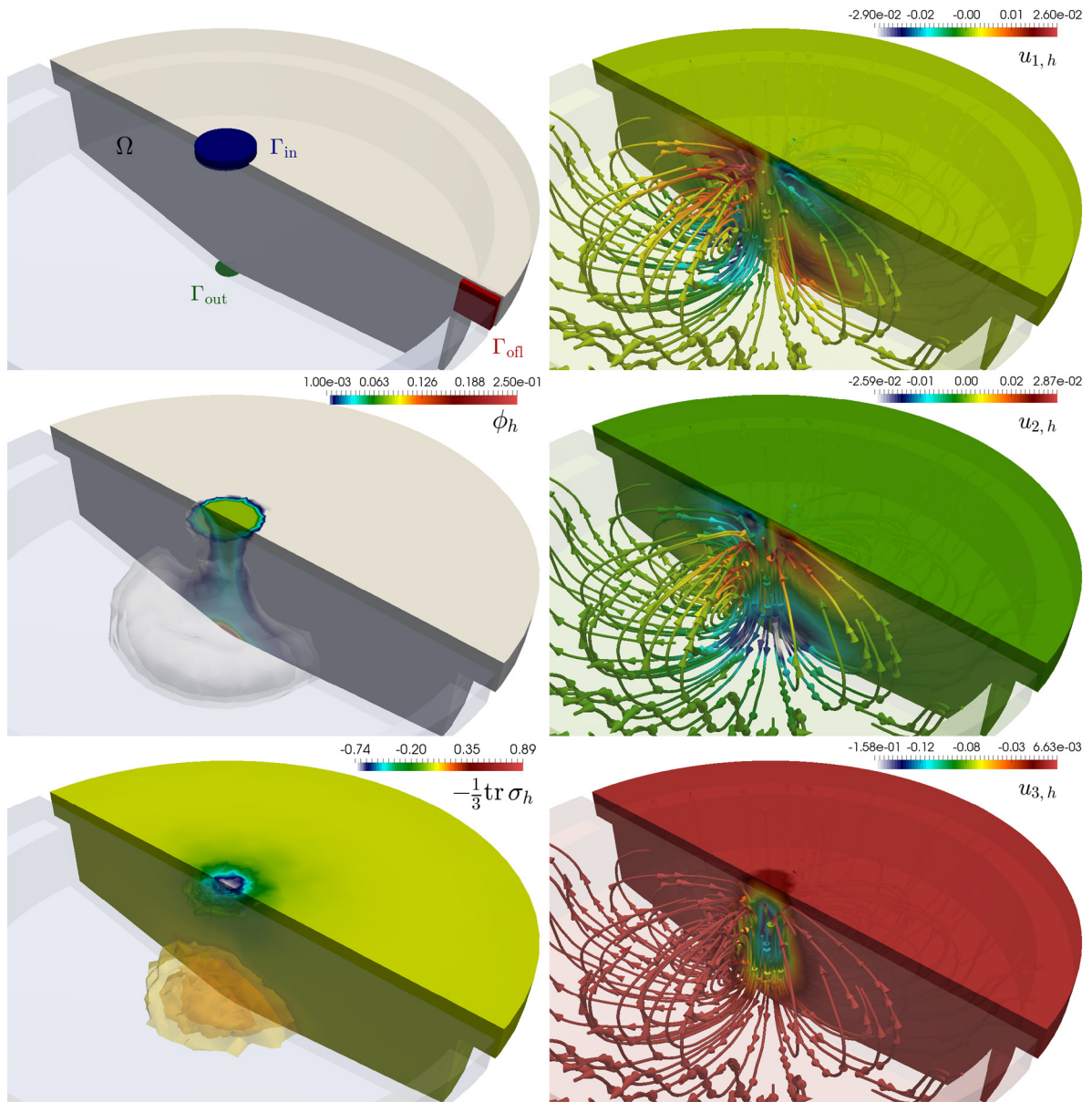


Fig. 6.5. Example 3. Sketch of the clipped domain and different boundaries in a clarifier-thickener device (top left panel), and snapshots of the approximate concentration, postprocessed pressure, and velocity components and streamlines computed with the proposed lowest order mixed-primal method.

velocity), whereas adaptive refinement according to the error estimator (4.2) restores optimal convergences and produces effectivity indexes that, even if are far from 1, do not oscillate. We also notice that for the maximum number of degrees of freedom, each individual error produced by the adaptive method is of about 10% of the errors generated with the method that uses quasi-uniform refinement, and also the Picard iteration count is slightly smaller.

6.3. Example 3: sedimentation in a clarifier-thickener unit

Next we present a numerical test that illustrates the performance of the proposed numerical scheme and the first *a posteriori* error indicator (5.1) on a 3D computation. The example reproduces the steady-state of a sedimentation–consolidation process in a clarifier-thickener unit. Model parameters and domain configuration are adapted from those in [5, Example 3], but here the device has a radial length of 14.6 m and a total height of 7.6 m. It features a feed inlet Γ_{in} consisting of an horizontal disk of radius 1.5 m, an underflow outlet for the discharge of sediment Γ_{out} (an horizontal disk of smaller radius 0.5 m), and a peripheral overflow annular region Γ_{off} (see a sketch in the top left panel of Fig. 6.5). A suspension is fed through Γ_{in} with velocity $\mathbf{u} = \mathbf{u}_{\text{in}} = (0, 0, -u_{3,\text{in}})^T$ and having a concentration of $\phi = \phi_{\text{in}}$. At the outlet Γ_{out} we set

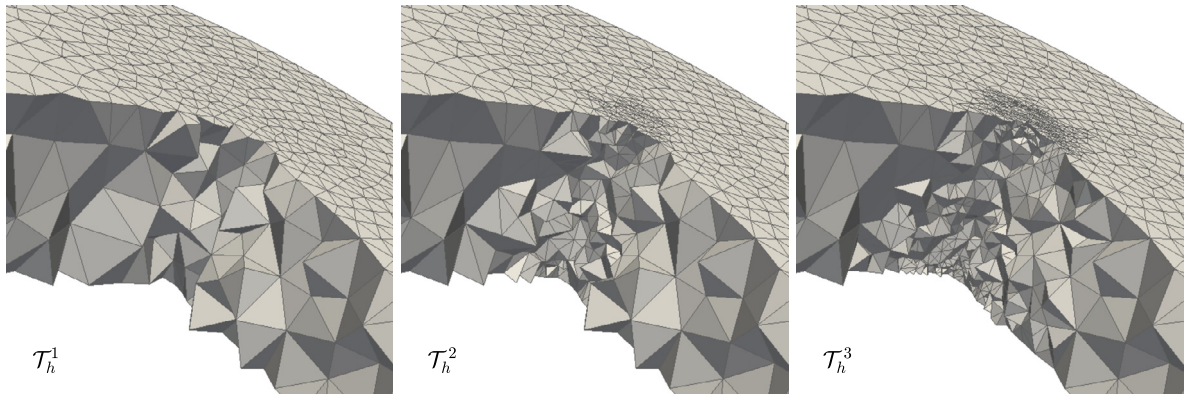


Fig. 6.6. Example 3. Zoom on the produced meshes after the first three steps of adaptive refinement using the first estimator as defined in (5.1).

$\mathbf{u} = \mathbf{u}_{\text{out}} = (0, 0, -u_{3,\text{out}})^T$; at the overflow annulus we impose zero normal pseudo-stresses; and on the remainder of $\partial\Omega$ we put no slip boundary data for the velocity and zero-flux conditions for the concentration.

The concentration-dependent coefficients are defined as in (6.2), and the remaining parameters are chosen as in Example 2, except for $u_{3,\text{in}} = 1.25\text{e-}2$, $u_{3,\text{out}} = 1.25\text{e-}3$, $\phi_c = 0.1$, $u_\infty = 2.2\text{e-}3$, $\phi_{\text{in}} = 0.08$, $\sigma_0 = 5.5\text{e-}2$, and $\beta = 1\text{e-}3$. Again, the bounds for the concentration imply that the stabilisation parameters assume the following values $\kappa_1 = 0.256$, $\kappa_2 = 0.25$.

The proposed primal-mixed method is used to generate the approximate solutions depicted in Fig. 6.5 (where we show only half of the domain, for visualisation purposes). As in [5,16], we can observe that the mixture concentrates near the outlet boundary Γ_{out} . The velocity arrows show recirculating patterns, and a very small underflow. In contrast with Example 2, here the Picard iterations until convergence are embedded inside the adaptive refinement loop, consisting of solving, estimating, marking and refining using the error equi-distribution strategy mentioned above. The plots in Fig. 6.6 show a sequence of three adapted meshes, forming a clustering of elements near the zones of high concentration gradients (connecting inflow and underflow boundaries), where also the velocity and postprocessed pressure profiles are more pronounced.

6.4. Scaling of the unknowns and of the estimators

For general coupled flow-transport problems, the reliability and efficiency constants may be unit-dependent. This issue could be remediated by defining parameters that contribute to enforce dimensional consistency among the terms that constitute the local error estimators, or simply by redefining problem (2.1) in its dimensionless form. For instance, let us define the adimensional velocity, Cauchy pseudo-stress, and differential operators as

$$\mathbf{u}^* = \mathbf{u}/V, \quad \boldsymbol{\sigma}^* = \boldsymbol{\sigma}/(\rho L^2), \quad \text{div} = \text{div}/L, \quad \nabla^* = \nabla/L,$$

where L denotes the space characteristic length of the domain, $V = L/T$ is a characteristic velocity where T is a characteristic time, and ρ is the characteristic density. As ϕ is already dimensionless (volume fraction), we see that the momentum equation for the flow problem and the transport equation can be recast in adimensional form. Making abuse of notation (that is, dropping the * superscript), the system reads

$$\begin{aligned} \widehat{\mathbf{K}}^{-1} \mathbf{u} - \text{div} \boldsymbol{\sigma} &= \widehat{\mathbf{f}} \phi, \\ \widehat{\beta} \phi - \text{div}(\vartheta(\phi) \nabla \phi) - \phi \mathbf{u} - \widehat{f}_{\text{bk}}(\phi) \mathbf{k} &= \widehat{\mathbf{g}}, \end{aligned}$$

where $\widehat{\mathbf{K}} = \mathbf{K}/L^2$, $\widehat{\mathbf{f}} = T/V \mathbf{f}$, $\widehat{\beta} = L^2 \beta$, $\widehat{f}_{\text{bk}}(s) = L f_{\text{bk}}(s)$, $\widehat{\mathbf{g}} = L^2 \mathbf{g}$ are the rescaled adimensional coefficients (see for instance [39]). The construction of the mixed-primal method and the analysis of the *a posteriori* error indicators follows then exactly as done in Sections 3–5.

It turns out that in Example 1, the constants involved in (6.1), the size of the domain, the model coefficients, and the constructed forcing and source terms, scale in such a way that they contribute to generating effectivity and quasi-effectivity indexes very close to one. This is no longer the case for Example 2 (see Table 2), as the scaling coefficients between the flow and transport terms (and subsequently their intrinsic weights into the local error indicators) differ by several orders of magnitude. This also implies that the adaptive refinement seen in Fig. 6.4 seems to be dictated by the velocity variations rather than by the stress or concentration patterns. Especially in the case of sedimentation–consolidation problems, one expects concentration solutions exhibiting sharp gradients while producing smooth flow profiles. We can then resort to a different scaling approach (which can be used together or independently of the adimensionalisation discussed above). Taking the second *a posteriori* error indicator (4.2) as an example, we can define

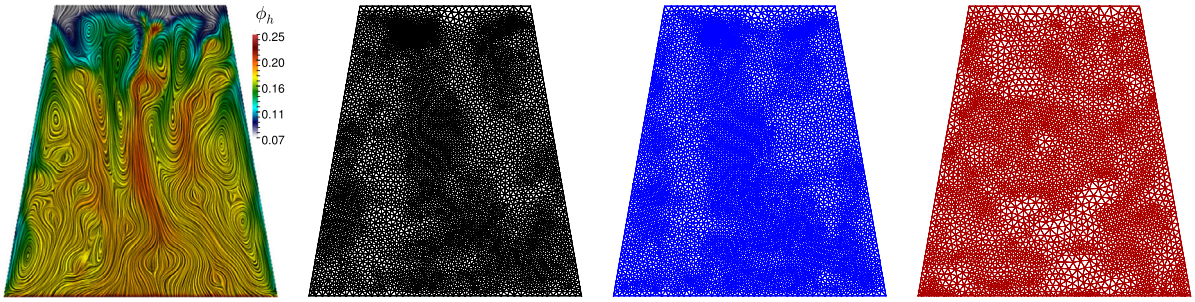


Fig. 6.7. Example 4. Sample of the computed concentration displayed on a line convolution integral driven by the discrete velocity (left) and adapted meshes after 5 steps, generated following the scaled estimator (6.3) and using the scaling factors $\widehat{M}^t = \widehat{M}^f = 1$ (middle left panel), $\widehat{M}^t = 100$, $\widehat{M}^f = 1$ (middle right panel), and $\widehat{M}^t = 5000$, $\widehat{M}^f = 0.1$ (right).

$$\begin{aligned} \widehat{\xi}_T^2 := & \widehat{M}^f \|\mathbf{f}\phi_h - \mathbf{K}^{-1}\mathbf{u}_h + \mathbf{div}\sigma_h\|_{0,T}^2 + \widehat{M}^f \|\nabla\mathbf{u}_h - [\mu(\phi_h)]^{-1}\sigma_h^d\|_{0,T}^2 + \widehat{M}^t h_T^2 \|g - \beta\phi_h + \mathbf{div}\tilde{\sigma}_h\|_{0,T}^2 \\ & + \widehat{M}^t \sum_{e \in \mathcal{E}_h(T) \cap \mathcal{E}_h(\Omega)} h_e \|\llbracket \tilde{\sigma}_h \cdot \mathbf{v}_e \rrbracket\|_{0,e}^2 + \widehat{M}^t \sum_{e \in \mathcal{E}_h(T) \cap \mathcal{E}_h(\Gamma_N)} h_e \|\tilde{\sigma}_h \cdot \mathbf{v}\|_{0,e}^2 + \widehat{M}^f \sum_{e \in \mathcal{E}_h(T) \cap \mathcal{E}_h(\Gamma_D)} \|\mathbf{u}_D - \mathbf{u}_h\|_{0,e}^2, \end{aligned} \quad (6.3)$$

and we have the liberty to modulate the scaling factors $\widehat{M}^t > 0$, $\widehat{M}^f > 0$ depending on whether a more important contribution to the error is expected from the concentration transport equation, or from the flow equations. Doing so, also allows one to trace back the dependence of the reliability and efficiency constants and consequently of the effectivity indexes (all being now dimensionless) on the scaling factors. However, we stress that even if these factors have the flexibility to include either dimensional or adimensional units, the reliability and efficiency bounds will still depend on constants that cannot be easily determined.

We exemplify the latter approach by redoing Example 2, now using (6.3) with different values for the scaling factors \widehat{M}^t and \widehat{M}^f . The adaptive mesh refinement five steps is shown in Fig. 6.7, which indicates a more clear clustering of elements near the zones of high concentration gradients when the ratio $\widehat{M}^t/\widehat{M}^f$ is larger.

Appendix A

A.1. Proof of Lemma 3.3

We begin by recalling, from [2, Lemma 3.4], that the bilinear form

$$A_{\phi,\mathbf{u}}(\varphi, \psi) := \int_{\Omega} \vartheta(\phi) \nabla\varphi \cdot \nabla\psi - \int_{\Omega} \varphi \mathbf{u} \cdot \nabla\psi + \int_{\Omega} \beta\varphi\psi \quad \forall \varphi, \psi \in H_{\Gamma_D}^1(\Omega), \quad (A.1)$$

is $H_{\Gamma_D}^1(\Omega)$ -elliptic with constant $\tilde{\alpha} := \frac{\vartheta_1}{2c_p}$, from which we deduce the following global inf-sup condition

$$\tilde{\alpha} \|\varphi\|_{1,\Omega} \leq \sup_{\substack{\psi \in H_{\Gamma_D}^1(\Omega) \\ \psi \neq 0}} \frac{A_{\phi,\mathbf{u}}(\varphi, \psi)}{\|\psi\|_{1,\Omega}} \quad \forall \varphi \in H_{\Gamma_D}^1(\Omega). \quad (A.2)$$

Next, applying (A.2) to the Galerkin error $\varphi := \phi - \phi_h$, we find that

$$\tilde{\alpha} \|\phi - \phi_h\|_{1,\Omega} \leq \sup_{\substack{\psi \in H_{\Gamma_D}^1(\Omega) \\ \psi \neq 0}} \frac{A_{\phi,\mathbf{u}}(\phi, \psi) - A_{\phi,\mathbf{u}}(\phi_h, \psi)}{\|\psi\|_{1,\Omega}}. \quad (A.3)$$

Now, using the fact that $A_{\phi,\mathbf{u}}(\phi, \psi) = A_{\mathbf{u}}(\phi, \psi) = G_{\phi}(\psi)$, and adding and subtracting suitable terms, it follows that

$$A_{\phi,\mathbf{u}}(\phi, \psi) - A_{\phi,\mathbf{u}}(\phi_h, \psi) = G_{\phi}(\psi) - G_{\phi_h}(\psi) + G_{\phi_h}(\psi) - A_{\mathbf{u}_h}(\phi_h, \psi) + A_{\mathbf{u}_h}(\phi_h, \psi) - A_{\phi,\mathbf{u}}(\phi_h, \psi). \quad (A.4)$$

In turn, using the definition of $A_{\mathbf{u}_h}$ (cf. (2.7)) and $A_{\phi,\mathbf{u}}$ (cf. (A.1)), we find that

$$\begin{aligned} A_{\mathbf{u}_h}(\phi_h, \psi) - A_{\phi,\mathbf{u}}(\phi_h, \psi) &= \int_{\Omega} (\vartheta(\phi) - \vartheta(\phi_h)) \nabla(\phi - \phi_h) \cdot \nabla\psi \\ &+ \int_{\Omega} \phi_h (\mathbf{u} - \mathbf{u}_h) \cdot \nabla\psi - \int_{\Omega} (\vartheta(\phi) - \vartheta(\phi_h)) \nabla\phi \cdot \nabla\psi, \end{aligned} \quad (A.5)$$

from which, employing the upper bound of ϑ (cf. (2.3)), (3.1), and proceeding as in [2, eq. (5.13)–(5.14)] on the third term to the right-hand side of (A.5), we arrive at

$$|A_{\mathbf{u}_h}(\phi_h, \psi) - A_{\phi, \mathbf{u}}(\phi_h, \psi)| \leq \left\{ 2\vartheta_2 + C_3 \left(\gamma_2 |\Omega|^{1/2} |\mathbf{k}| + \|g\|_{\delta, \Omega} \right) \right\} \|\phi - \phi_h\|_{1, \Omega} |\psi|_{1, \Omega} + r c(\Omega) \|\mathbf{u} - \mathbf{u}_h\|_{1, \Omega} |\psi|_{1, \Omega}. \tag{A.6}$$

Thus, applying the estimate for $|G_{\phi}(\psi) - G_{\phi_h}(\psi)|$ (see [2, eq. (5.12)]) and estimate (A.6), we obtain from (A.3) and (A.4) that

$$\|\phi - \phi_h\|_{1, \Omega} \leq \tilde{C} \|G_{\phi_h} - A_{\mathbf{u}_h}(\phi_h, \cdot)\|_{H^1_{\Gamma_D}(\Omega)'} + \left\{ C_4 |\mathbf{k}| + C_5 \|g\|_{\delta, \Omega} + C_6 \vartheta_2 \right\} \|\phi - \phi_h\|_{1, \Omega} + r c(\Omega) \tilde{C} \|\mathbf{u} - \mathbf{u}_h\|_{1, \Omega}.$$

Then, bounding $\|\mathbf{u} - \mathbf{u}_h\|_{1, \Omega}$ by the error estimate provided by (3.8) (cf. Lemma 3.2), and employing (3.13), we deduce that

$$\|\phi - \phi_h\|_{1, \Omega} \leq 2\tilde{C} \left\{ \|G_{\phi_h} - A_{\mathbf{u}_h}(\phi_h, \cdot)\|_{H^1_{\Gamma_D}(\Omega)'} + C_9 \left(\theta_0 + \|E_h\|_{\mathbb{H}_N(\mathbf{div}, \Omega)'} \right) \right\}, \tag{A.7}$$

where, bearing in mind (3.15), there holds

$$G_{\phi_h} - A_{\mathbf{u}_h}(\phi_h, \cdot) = \tilde{E}_h,$$

and hence (A.7) yields (3.14). Finally, using the fact that $G_{\phi_h}(\psi_h) - A_{\mathbf{u}_h}(\phi_h, \psi_h) = 0 \quad \forall \psi_h \in H^\phi_h$, we obtain (3.16) and the proof concludes.

A.2. Proof of Lemma 3.18

The estimates given in (3.39) were established in [3, eq. (3.71)–(3.72)]. On the other hand, using the Lipschitz continuity assumption on ϑ (cf. (2.4)), but restricted to each triangle $T \in \mathcal{T}_h$ instead of Ω , employing Cauchy–Schwarz’s inequality and the compactness (and hence continuity) of the injection $i : H^1(\Omega) \rightarrow L^4(\Omega)$ (cf. [1, Theorem 6.3]), we deduce that

$$\begin{aligned} \sum_{T \in \mathcal{T}_h} \|(\vartheta(\phi) - \vartheta(\phi_h)) \nabla \phi\|_{0, T}^2 &\leq \sum_{T \in \mathcal{T}_h} L_\vartheta^2 \|\phi - \phi_h\|_{L^4(T)}^2 \|\nabla \phi\|_{L^4(T)}^2 \\ &\leq L_\vartheta^2 \|\phi - \phi_h\|_{L^4(\Omega)}^2 \|\nabla \phi\|_{L^4(\Omega)}^2 \leq \tilde{c}_9 \|\phi - \phi_h\|_{1, \Omega}^2, \end{aligned}$$

where \tilde{c}_9 depends only on $\|i\|$, L_ϑ , and $\|\nabla \phi\|_{L^4(\Omega)}$, which gives (3.40) and finishes the proof.

References

- [1] R.A. Adams, J.J.F. Fournier, Sobolev Spaces, Academic Press, Elsevier Ltd, 2003.
- [2] M. Alvarez, G.N. Gatica, R. Ruiz-Baier, A mixed-primal finite element approximation of a sedimentation–consolidation system, Math. Models Methods Appl. Sci. 26 (5) (2016) 867–900.
- [3] M. Alvarez, G.N. Gatica, R. Ruiz-Baier, A posteriori error analysis for a viscous flow-transport problem, ESAIM: Math. Model. Numer. Anal. 50 (6) (2016) 1789–1816.
- [4] M. Alvarez, G.N. Gatica, R. Ruiz-Baier, A posteriori error analysis of a fully-mixed formulation for the Brinkman–Darcy problem, Calcolo 54 (4) (2017) 1491–1519.
- [5] M. Alvarez, G.N. Gatica, R. Ruiz-Baier, An augmented mixed-primal finite element method for a coupled flow-transport problem, ESAIM: Math. Model. Numer. Anal. 49 (5) (2015) 1399–1427.
- [6] C. Amrouche, C. Bernardi, M. Dauge, V. Girault, Vector potentials in three-dimensional nonsmooth domains, Math. Methods Appl. Sci. 21 (1998) 823–864.
- [7] V. Anaya, M. Bendahmane, D. Mora, R. Ruiz-Baier, On a vorticity-based formulation for reaction–diffusion–Brinkman systems, Netw. Heterog. Media 13 (1) (2018) 69–94.
- [8] I. Babuška, G.N. Gatica, A residual-based a posteriori error estimator for the Stokes–Darcy coupled problem, SIAM J. Numer. Anal. 48 (2) (2010) 498–523.
- [9] C. Bernardi, L. El Alaoui, Z. Mghazli, A posteriori analysis of a space and time discretization of a nonlinear model for the flow in partially saturated porous media, IMA J. Numer. Anal. 34 (3) (2014) 1002–1036.
- [10] F. Betancourt, R. Bürger, R. Ruiz-Baier, H. Torres, C.A. Vega, On numerical methods for hyperbolic conservation laws and related equations modelling sedimentation of solid-liquid suspensions, in: G.-Q. Chen, H. Holden, K.H. Karlsen (Eds.), Hyperbolic Conservation Laws and Related Analysis with Applications, Springer-Verlag, Berlin, 2014, pp. 23–68.
- [11] M. Braack, T. Richter, Solving multidimensional reactive flow problems with adaptive finite elements, in: Reactive Flows, Diffusion and Transport, Springer, Berlin, 2007, pp. 93–112.
- [12] F. Brezzi, M. Fortin, Mixed and Hybrid Finite Element Methods, Springer-Verlag, 1991.
- [13] R. Bürger, J. Careaga, S. Diehl, C. Mejías, R. Ruiz-Baier, Convection–diffusion–reaction and transport-flow problems motivated by models of sedimentation: some recent advances, Proc. Int. Cong. Math. 1 (2018) 21–30.
- [14] R. Bürger, S. Kumar, S.K. Kenettinkara, R. Ruiz-Baier, Discontinuous approximation of viscous two-phase flow in heterogeneous porous media, J. Comput. Phys. 321 (2016) 126–150.
- [15] R. Bürger, S. Kumar, R. Ruiz-Baier, Discontinuous finite volume element discretization for coupled flow-transport problems arising in models of sedimentation, J. Comput. Phys. 299 (2015) 446–471.

- [16] R. Bürger, R. Ruiz-Baier, H. Torres, A stabilized finite volume element formulation for sedimentation–consolidation processes, *SIAM J. Sci. Comput.* 34 (3) (2012) B265–B289.
- [17] C. Carstensen, A posteriori error estimate for the mixed finite element method, *Math. Comput.* 66 (218) (1997) 465–476.
- [18] C. Carstensen, G. Dolzmann, A posteriori error estimates for mixed FEM in elasticity, *Numer. Math.* 81 (2) (1998) 187–209.
- [19] P. Clément, Approximation by finite element functions using local regularization, *RAIRO Model. Math. Anal. Numér.* 9 (2) (1975) 77–84.
- [20] D.A. Di Pietro, E. Flauraud, M. Vohralík, S. Yousef, A posteriori error estimates, stopping criteria, and adaptivity for multiphase compositional Darcy flows in porous media, *J. Comput. Phys.* 276 (2014) 163–187.
- [21] C. Domínguez, G.N. Gatica, S. Medahi, A posteriori error analysis of a fully-mixed finite element method for a two-dimensional fluid–solid interaction problem, *J. Comput. Math.* 33 (6) (2015) 606–641.
- [22] A.I. Garralda-Guillen, G.N. Gatica, A. Márquez, M. Ruiz, A posteriori error analysis of twofold saddle point variational formulations for nonlinear boundary value problems, *IMA J. Numer. Anal.* 34 (1) (2014) 326–361.
- [23] G.N. Gatica, A note on the efficiency of residual-based a-posteriori error estimators for some mixed finite element methods, *Electron. Trans. Numer. Anal.* 17 (2004) 218–233.
- [24] G.N. Gatica, *A Simple Introduction to the Mixed Finite Element Method: Theory and Applications*, Springer Briefs Math., Springer, Cham, 2014.
- [25] G.N. Gatica, A note on stable Helmholtz decompositions in 3D, Preprint 2016-03, Centro de Investigación en Ingeniería Matemática (CI²MA), Universidad de Concepción, Chile, 2016, available from <http://www.ci2ma.udec.cl>.
- [26] G.N. Gatica, L.F. Gatica, A. Márquez, Analysis of a pseudostress-based mixed finite element method for the Brinkman model of porous media flow, *Numer. Math.* 126 (4) (2014) 635–677.
- [27] G.N. Gatica, L.F. Gatica, F.A. Sequeira, A priori and a posteriori error analyses of a pseudostress-based mixed formulation for linear elasticity, *Comput. Math. Appl.* 71 (2) (2016) 585–614.
- [28] G.N. Gatica, A. Márquez, M.A. Sánchez, Analysis of a velocity–pressure–pseudostress formulation for the stationary Stokes equations, *Comput. Methods Appl. Mech. Eng.* 199 (17–20) (2010) 1064–1079.
- [29] G.N. Gatica, A. Márquez, M.A. Sánchez, A priori and a posteriori error analysis of a velocity–pseudostress formulation for a class of quasi-Newtonian Stokes flows, *Comput. Methods Appl. Mech. Eng.* 200 (17–20) (2011) 1619–1636.
- [30] V. Girault, P.A. Raviart, *Finite Element Methods for Navier–Stokes Equations. Theory and Algorithms*, Springer-Verlag, Berlin, 1986.
- [31] M.G. Larson, A. Målqvist, Goal oriented adaptivity for coupled flow and transport problems with applications in oil reservoir simulations, *Comput. Methods Appl. Mech. Eng.* 196 (37–40) (2007) 3546–3561.
- [32] M.G. Larson, R. Söderlund, F. Bengzon, Adaptive finite element approximation of coupled flow and transport problems with applications in heat transfer, *Int. J. Numer. Methods Fluids* 57 (9) (2008) 1397–1420.
- [33] P. Lenarda, M. Paggi, R. Ruiz-Baier, Partitioned coupling of advection–diffusion–reaction systems and Brinkman flows, *J. Comput. Phys.* 344 (2017) 281–302.
- [34] J.E. Roberts, J.M. Thomas, Mixed and hybrid methods, in: P.G. Ciarlet, J.L. Lions (Eds.), *Handbook of Numerical Analysis*, vol. II, Finite Elements Methods (Part 1), North-Holland, Amsterdam, 1991.
- [35] R. Ruiz-Baier, I. Lunati, Mixed finite element–discontinuous finite volume element discretization of a general class of multicontinuum models, *J. Comput. Phys.* 322 (2016) 666–688.
- [36] R. Ruiz-Baier, H. Torres, Numerical solution of a multidimensional sedimentation problem using finite volume–element methods, *Appl. Numer. Math.* 95 (1) (2015) 280–291.
- [37] U. Schaffinger, Experiments on sedimentation beneath downward-facing inclined walls, *Int. J. Multiph. Flow* 11 (1) (1985) 189–199.
- [38] S. Sun, M.F. Wheeler, Local problem-based a posteriori error estimators for discontinuous Galerkin approximations of reactive transport, *Comput. Geosci.* 11 (2) (2007) 87–101.
- [39] V.A. Vanoni, *Sedimentation Engineering: American Society of Civil Engineers, Manuals and Reports on Engineering Practice*, no. 54, 1975.
- [40] R. Verfürth, A posteriori error estimation and adaptive–mesh–refinement techniques, *J. Comput. Appl. Math.* 50 (1–3) (1994) 67–83.
- [41] R. Verfürth, *A Review of A Posteriori Error Estimation and Adaptive–Mesh–Refinement Techniques*, Wiley–Teubner, Chichester, 1996.
- [42] M. Vohralík, M.F. Wheeler, A posteriori error estimates, stopping criteria, and adaptivity for two-phase flows, *Comput. Geosci.* 17 (5) (2013) 789–812.